ABSTRACT

KRISHNAN, ARVIND SIVARAMA. Using Michell Truss Principles to find an Optimal Structure Suitable for Additive Manufacturing. (under the direction of Dr. John Strenkowski.)

Additive Manufacturing (AM) technology is improving its capabilities in terms of precision, variety of materials available, build time and mechanical properties of the final part. Due to the nature of the process, the time required to manufacture a design is only dependent on its dimensions and independent of the complexity of the geometry. It is now used for rapid manufacturing in aerospace and biomedical applications and other industries as well. Michell truss inspired optimum designs, which are complex to manufacture through traditional methods, can now be made using AM technology. In this thesis, a new method for finding the internal lattice of a Michell truss is introduced using a finite element analysis. For a simply-supported beam, the internal shape is defined and an algorithm is used to optimize the geometry taking AM constraints into account and the results are compared with existing published data. Once the method is validated, the same procedure is applied to a cantilever beam with a point end load. The internal lattice is defined and an optimization algorithm is used to find the minimum required thickness of all struts to achieve a minimum weight beam.

Using Michell Truss Principles to find an Optimal Truss Structure Suitable for Additive Manufacturing

by
Arvind Sivarama Krishnan

A thesis submitted to the Graduate Faculty of
North Carolina State University
in partial fulfillment of the
requirements for the degree of
Master of Science

Mechanical Engineering

Raleigh, North Carolina

2015

APPROVED BY:

_____	_____
Dr. Scott Ferguson	Dr. Kara Peters

_____

Dr. John Strenkowski
Chair of Advisory Committee

BIOGRAPHY

Arvind Krishnan was born in Doha, Qatar on February 28th, 1989 and grew up in Mumbai, India. In 2005, his family moved to Austin, Texas where he studied at West Lake High School. He completed his Bachelors of Science in Mechanical Engineering with high honors from the University of Texas at Arlington. Then, he worked at GoEngineer as a Simulation Technical Support Engineer for a couple of years.

Following this, Arvind moved to Raleigh, North Carolina to pursue his graduate studies at the North Carolina State University beginning August 2013. During the summer of 2014, he interned at *The Gigtank* in Chattanooga, TN. Working as an Additive Manufacturing Specialist, Arvind worked on multiple projects in collaboration with multiple 3D-Printing start-up companies.

Arvind enjoys playing Tennis, Badminton, Racquetball, Chess and Soccer. He is also passionate about hiking and cooking.

ACKNOWLEDGEMENTS

I would like to thank Dr. John Strenkowski for giving me the opportunity to work under his guidance during my research. You have been open to new ideas and always had the bigger picture in mind. Thank you Dr. Peters and Dr. Ferguson for being part of my committee and providing valuable inputs.

I would not be here today without my amazing parents. Amma, you have sacrificed so much and constantly catered to my unending needs. Appa, you have been my best friend, mentor and protector at all times. My brother Anand has always been there to cover up when I got into trouble with my continuous mischief. With you all by my side, no challenge seems daunting, no task impossible and no mountain is too tall to climb. To my family, including Kirti, thank you for the constant support.

My mentors Dr. Hyejin Moon, Dr. Kamesh Subbarao, Srinivas Krishnan, and Brad Hansen, thank you for your continuous guidance during pivotal moments in my career.

To my undergraduate friends: Channa, Abhilash, Isura, Sunny, and Andie, here is to all the crazy and irreplaceable memories, to the countless arguments about religion and politics, plans to take over big companies, endless parties and family-like support. Thank you all.

Graduate school has been a crazy ride thanks to the awesome people of *Chai Khaana Vagera* (Tea, Snacks etcetera). The memories of coming home after a long day of work to tea made in a cooker and fifteen people laughing at funny YouTube videos are etched into my

memory. A special note of appreciation to Subramaniam Iyer and Navneet Arakony, for always caring and being there at all times.

Last, but not least, I'd like to mention Nikhil Shrivatsan, Ketan Shende, Shengqi Zhang and Rohit Pagedar for helping me with the optimization algorithm, Arunachalam Thiravium for valuable inputs on Michel truss layouts, and my optimization project group.

TABLE OF CONTENTS

LIST OF TABLES

LIST OF FIGURES

1. INTRODUCTION

Over the past thirty years, three-dimensional (3D) printers have gained prominence as an integral component in the design to manufacturing process. In this method, a CAD model is additively manufactured one layer at a time using a 3D printer. Due to the nature of the process, the time, cost and material required to manufacture a part is only dependent on its dimensions and independent of the complexity of the geometry.

Originally, this technology was used mainly for prototyping purposes. However, with improvements in various aspects of the technology like speed, material properties and cost of production, there has been a gradual switch towards more end products and customized designs which allow this technology to be used by a more diverse range of people (1). One such customized design of a chair can be seen in Figure 1.1 below (1).

Figure 1.1 Custom Chair Design

As expected, there are many engineering applications that can benefit from additive manufacturing. Doubrovski (2) stated that the principal objective of engineering is to develop

the stiffest structure possible by using the least amount of material. Michell (3) laid the foundations for such a structure by saying that all elements must follow paths of maximum strain so that the topology is the stiffest for a given mass.

The resulting topology from such a structure is too complex for traditional manufacturing techniques. However, with the use of additive manufacturing, it is now possible to design such structures with no additional cost or time. In the past, design for manufacturing guidelines would dictate that parts be kept simple so that manufacturing process requirements such as draft angles and wall thickness could be adhered to. With this new technology, parts can be made with greater complexity, and process considerations are less prominent (4). There is a clear need for a methodology to optimize the creation of complex shapes while taking the requirements of an additive manufacturing process into consideration.

The objective of this thesis is to create a topology optimized design using a Michell truss layout while also accounting for additive manufacturing constraints. The design freedom provided by additive manufacturing (AM) will be utilized in designing a minimum weight lattice structure. A brief background of the additive manufacturing industry, Michell trusses, and optimization procedures is first described. The internal lattice of a simply-supported beam is determined using a Michell truss as the basis of the structure. The mass of the truss is minimized by optimizing the thickness of each strut in the truss and then it is compared with an existing optimized design. The optimization algorithm used is called Simulated Annealing which is a commonly used heuristic technique.

A second example is provided of a Michell truss layout of a cantilever beam with a point load. Although the additive manufacturing process affords new design freedom as compared with more traditional manufacturing methods, it also requires that additional constraints be satisfied. These constraints are described in the thesis and included in the algorithm for manufacturing real parts. The algorithm and constraints described in this thesis are general and they can be used for any AM technology, printer, or material.

2. ADDITIVE MANUFACTURING INDUSTRY

2.1 Description and History

The industrial revolution paved the way to manufacture one part repetitively using production lines. Men and woman operate highly automated machinery using a computer and manufacturing facilities to produce parts (5). However, this approach is not cost effective if a single part with a customized design is required. Manufacturers would need to invest in tooling, casting and a unique suitable finishing technique. It would costs thousands of dollars just to create one unique customized design (5). This is where additive manufacturing proves useful.

Figure 2.1 Cube 3 Printer from 3D Systems (6)

The 3D printing or additive manufacturing industry started with Chuck Hull who filed a patent in 1986 for using Stereolithography to solidify a thin layer of liquid plastic and repeated the process by adding more plastic (6). He went on to start 3D Systems, a successful

3D printer manufacturer company, while other innovators used the concept of solidifying one layer at a time to create new AM techniques and 3D printers. Figure 2.1 above shows a 3D printer currently manufactured by 3D Systems.

The mechanical properties of the final part are dependent on which additive manufacturing process is used and which options are selected for each of the parameters like speed of printer head and temperature. These mechanical properties are constantly evolving with time and research. The following sections briefly describe the different AM processes in use today and some of the current on-going research.

2.2 Current Research and Industry Usage

In 2009, a meeting of 65 experts in the additive manufacturing field released a document titled '2009 Roadmap for Additive Manufacturing'. The document gave recommendations on the direction of focus of research for the next few years in this field (7). Some recent research developments are highlighted here. The parameters that determine the properties of the finished part are:

- Purity of material used
- Mechanical properties of powder
- Printer head temperature relative to melting point of material
- Speed of the printer head, thickness of each layer, and
- Ambient conditions

There has been considerable research to improve performance of these parameters. Jariwala conducted a study on a process planning method with the ability to cure a film to various thicknesses (8). Recently, greater emphasis has been focused on freedom of design to manufacture parts, especially cellular structures, optimal designs and repeatable unit cells (9). As additive manufacturing becomes a more integral part of how things are made, there is research and development in supply chain management, and logistics for using additive manufacturing (9). Microstructural lattice design is another area that is gaining prominence. Recently, Krishnan Suresh developed a framework for the same, expecting increased manufacturing through 3D printers in the near future (10). Using this, the density of the lattice at different areas of a design can be altered based on the stress distribution, resulting in weight reduction.

Although it is a new technology, many people own something that has been 3D printed. This technology is also spreading to new markets. Customized foods of different shapes and designs like pancakes and cakes are being 3D printed for special occasions. Artists are using it to create 3D sculptures of varied complexity. Multiple start-ups and research institutes like 3D Ops and Formlabs are trying to make replications of human organs with 3D printers (11).

The aerospace industry manufactures complicated parts that must meet stringent design requirements for strength and weight, but does not usually have high production volumes. As a consequence, the aerospace industry has adopted AM technology for the production of many aircraft parts. As of 2012, Boeing produced more than 20,000 3D printed parts for ten different types of military and commercial airplanes including the new

Dreamliner which has about thirty 3D printed parts (12). General Electric (GE) recently used additive manufacturing to fabricate a leap engine that was successfully used in flight (13). GE Aviation estimates that the majority of their parts will be manufactured in this manner by 2020 (14).

2.3 Methods of Additive Manufacturing

In this section, the different methods of additive manufacturing are briefly reviewed. Electron Beam Melting (EBM) is primarily used for metals. For this process, a bed of pure metal powder is selectively melted using a powerful electron beam. The printer head is heated to the melting temperature of the feedstock material. Once a particular layer is melted based on CAD geometry, the bed is lowered, and a new layer of metal powder is rolled above the bed, and flattened. Then, the printer head again selectively melts another layer. Each layer is melted to the exact geometry as defined by a CAD model until the entire part is created (15). Arcam AB $^{(R)}$ is a Swedish company that produces machines using the EBM technology and prints finished parts that are used in many real world applications. Another similar technology used for metal printing is called Direct Metal Laser Sintering (DMLS). In this process, a laser is used to sinter the powder one layer at a time.

A technique commonly used for plastic parts is Fusion Deposition Modeling. A thermoplastic is heated to a semi-liquid state and deposited along the extrusion path as defined by a CAD model (16). In some machines, support material is added where needed and later removed. This process is very common and it is used by many startups to make 3D

printed parts. The feedstock plastic material used in this process comes in a variety of textures and mechanical properties.

Stereolithography is another commonly used technology where liquid resin is selectively hardened as defined by the desired geometry. A Boston-based startup company called Formlabs has developed printers using this technology. High precision can be achieved with these printers so they may be used to manufacture intricate parts (17).

2.4 Summary

As 3D printing becomes an intrinsic part of manufacturing, the topology of a design can undertake more and more complex shapes. Previously optimized topology designs that were considered too complicated to manufacture can now be made at no additional cost or time. From a design engineer's standpoint there are new and untapped possibilities. 3D printing provides the ability to use multiple materials at different areas of the design and creates a seamless transition from one material to the other. The next section reviews Michell trusses and how they create an optimum design layout.

3. REVIEW OF MICHELL TRUSSES

3.1 History of the Michell Truss

Topology optimization has been a central theme of engineering for many decades. In 1869, Clerk Maxwell described the amount of material needed to resist a set of compressive and tensile forces for a given framework (18). However, the theory had direct use only for tension and compression loads. Michell worked on Maxwell's theorem to generalize it for any displacement input. The basic goal of this layout is to transmit the forces to a point of support with minimal volume, without exceeding stress limits; the forces are point loads and the solution is discrete continuous (19).

In 1904, AGM Michell (3) described the stiffest structure for a given design by adding material along the paths of maximum strain magnitude. The optimization for minimum-weight was solely for 2D structures. Hence, only plane strain problems with constant cross sectional areas could be optimized as a Michell truss. He said that a frame attains the limit of economy of material possible under the same applied force. The feasible space consists of orthogonal systems of members in tension and compression. These members are called slip lines and will be discussed later in more detail. Michell's trusses were initially an inspiration for civil engineers for designing new shapes of buildings.

Figure 3.1 was used by Michell to explain the theory. The bolder continuous trajectories are in compression and the lighter continuous trajectories are in tension. These paths are called slip lines. Force 'F' at point A is balanced by a reaction moment at B of

value *F X length (AB)* Frames whose bars coincide with these curves will represent minimum quantity of material required. The dotted lines represent trajectories of principal strain where material bars are not required.

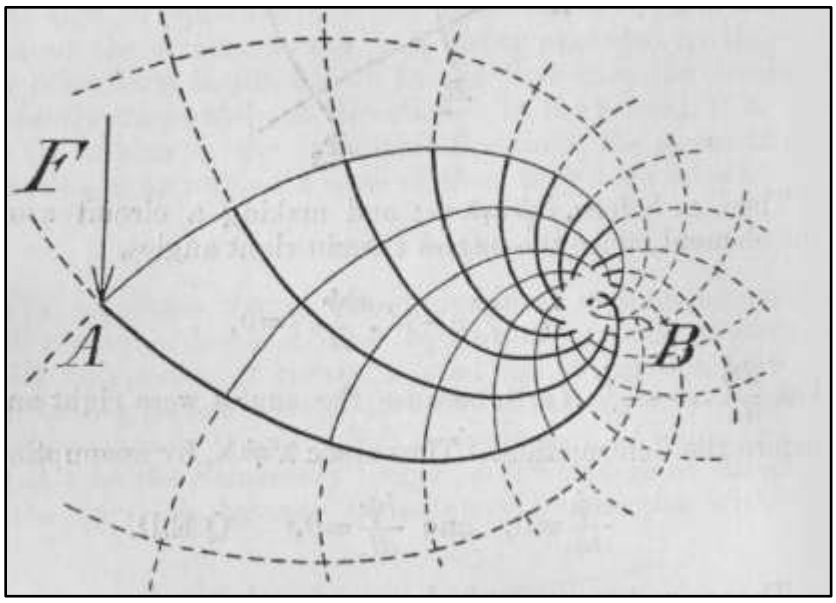

Figure 3.1 Michell Truss Layout

Michell's work was largely unnoticed for 50 years until Cox and Hemp realized the importance of his findings and developed it further. Cox found exact solutions for an optimization problem based on Michell's work and publish his findings in 1965 (20). Hemp was credited with finding a correlation between Michell's truss layout and the plastic deformation of metals during operations such as die casting (21). The trajectories of plastic deformation which naturally follow the path of least resistance coincide with these slip lines.

3.2 Slip Lines

The lines in the middle of the Michell truss layout in tension are called alpha lines and the ones in compression are called beta lines. Together, they are referred to as slip lines and they are shown in Figure 3.2. Alpha and beta lines are always perpendicular to each other at their points of intersection.

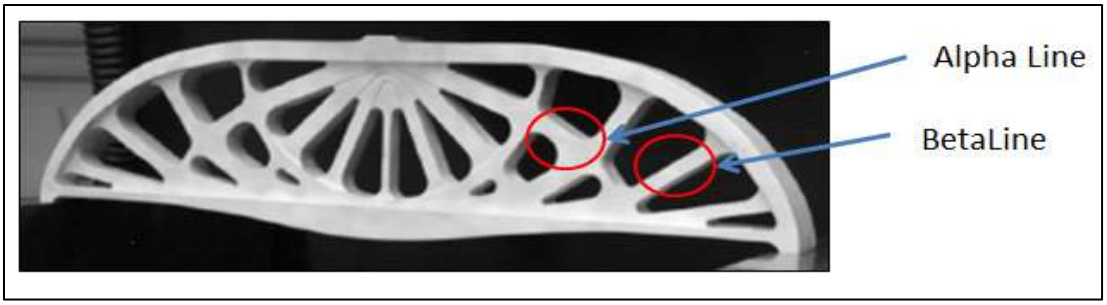

Figure 3.2 Alpha and Beta lines

Slip lines intersect the neutral axis at either a positive or negative angle of 45^{o}. Any number of slip lines can be used to describe a Michell truss layout. The coordinate system is created with alpha and beta lines such that the angle of tangential stress τ is positive. The angle of τ with respect to the alpha line is measured as θ. The relationship of θ with the curvature of alpha and beta lines are described as

Alpha Lines: $\frac{dy}{dx} = \tan\theta$ Beta Lines: $\frac{dy}{dx} = -\cot\theta$

3.3 Correlation with Other Fields

As described above, once a correlation was found between slip line fields and the lines of plastic deformation of metals, the interest in solving these topology problems grew. Hemp developed an analytical method to derive slip line fields, but in general, complex analytical expressions are needed especially when the geometry is not trivial.

It was found that these slip lines could be correlated with the plastic deformation field around a crack tip in the study of fracture mechanics as explained by Hutchinson in 1968 (22). He constructed a stress field centered at the crack tip. This field also had resemblance with slip line fields initially developed by Michell. Perfectly plastic behavior was assumed for these fields. Figure 3.3 below shows such a field for a plane strain case.

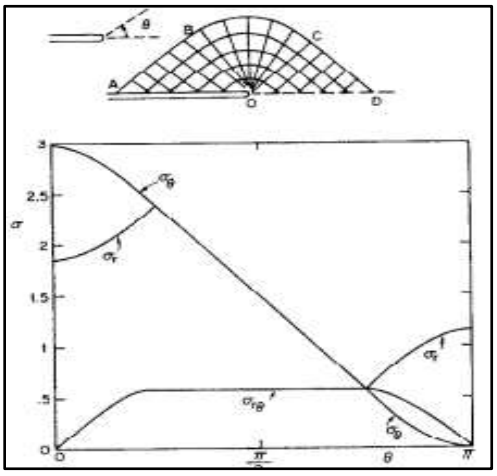

Figure 3.3 Stress Field for Perfectly Plastic Material (22)

During the 1960's, multiple numerical methods were derived to create slip line fields. This coincided with the advent of computers and increased computing power. J. F. Ewing developed a series method for constructing plastic slip line fields. He used a power series to numerically approximate the slip line field (23). He defined the radii of curvature across the field as a power series function of the different parameters and developed a numerical solution. It was found that inverting the resulting equations to find the unknown coefficient was difficult especially for complicated problems.

There is a small distinction in finding slip lines for optimum structures as opposed to finding them for plane strain deformations. As described by Dewhurst (24), in the plane strain metal deformation theory, the main area of focus was finding solutions to specific boundary value problems for commonly used tool geometries such as die casting. In contrast to designing structures with minimum weight, multiple examples can be developed for unrestricted optimum structures.

3.4 Michell Theory Shortcomings

In 1973, Hemp (25) described some modifications needed to Michell's theory and called them Michell's optimality criteria in honor of the original work. Also, Hemp assumed one permissible stress value for both compressive and tensile stresses. Examples of solutions in which different permissible stresses are present were not given. This was followed by Rozvany (2) demonstrated that Michell's criteria is valid for all support conditions only if the compressive and tensile permissible stresses are equal and if there is kinematic admissibility. For most materials, Michell's optimality conditions are valid merely for a restricted class of

support conditions. Also, statically indeterminate loading conditions do not conform to Michell's optimality criteria. Michell's truss exclusively optimizes two dimensional structures in a plane stress condition.

In this section, a brief history of Michell Trusses including a description of slip lines and their correlation with plastic strain was described including some of its shortcomings. The following section reviews recent work in the field of topology optimization including an introduction of several methods for achieving an optimal structural design.

4. REVIEW OF TOPOLOGY OPTIMIZATION

4.1 Categorizing Topology Optimization Methods

Topology optimization is the process of determining the connectivity, shape, and location of voids inside a given domain (26). In the last two decades, there has been rapid growth and continuous research in optimization techniques and it is an active area of research in the field of structural and multidisciplinary optimization. In structural optimization, there are a variety of different loading conditions. If the loading condition is similar to a pressure vessel, it is design-dependent as well. One of the difficulties in shape optimization is that the optimal shape may represent a multiply-connected set with internal boundaries whose topology is not known and is difficult to determine because new internal boundaries cannot be easily generated (27). There have also been exhaustive reviews conducted in this field. This section provides a brief overview and discusses some specific methods.

The various methods of topology optimization can be broadly classified into two specific groups as described by Srithongchai (28). The first is to change the size and layout of trusses for a given number of nodes to achieve a specific design objective. In this method, nodes that are too close to each other are merged together. Another approach couples a Finite Element Analysis (FEA) code such as ANSYS with an optimization procedure. Density values are modified based on the stress distributions. Regions of very low stress are removed from the design altogether.

The specific methods gaining recent popularity are density-based methods called Solid Isotropic Material and Penalization (SIMP) and Evolutional Structural Optimization

(ESO). Within a fixed domain, the goal of the optimization problem is to identify whether each element should contain a solid material or remain void (26). In most similar problems, the objective function will be a volume to stiffness ratio or compliance, and constraints are set on material usage and the physical model is represented in a discretized form. For this method, the algorithm is often coupled with an FEA code. Such optimization techniques have often resulted in a structure as shown in Figure 4.1 (29) as a discretized form. This specific example also considered traditional manufacturing constraints.

Figure 4.1 Discretized ESO Optimized Structure Shape (29)

In the previous method for density variation calculation, density was a discrete variable where each cell is either void or solid. Currently, research is being conducted using material models which allow the density of the material to cover a complete range from 0 (void) to 1 (solid) where all intermediate values are also acceptable (30). This can be achieved with a periodic perforated microstructural material whose density is a design variable that can change.

A bubble method was described by Eschenauer (31) about twenty years ago which is included under the ESO method. An iterative positioning and a hierarchically structured shape optimization for new holes were used. The boundaries were treated as parameters and the shape of new bubbles was determined as a parametric optimization. Figure 4.2 shows the initial design and the increasing size of the bubbles as it progresses towards the optimized design.

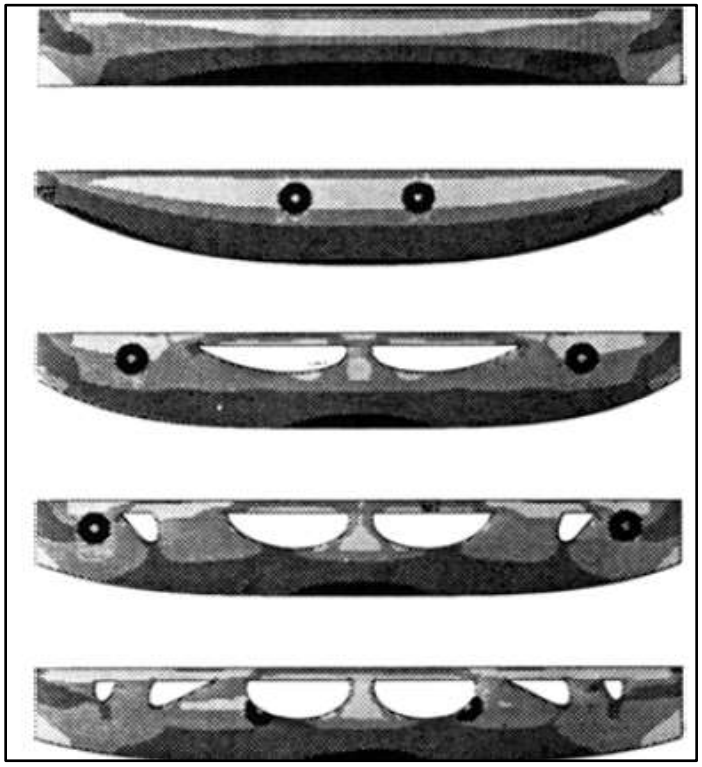

Figure 4.2 Topology Optimization by Bubble Method (31)

The method chosen for topology optimization also changes based on the application. Dentistry, biomedical, and aerospace applications have slight differences depending on whether they are structural or aeronautical applications.

4.2 Coupling Optimization Methods with a Finite Element Code

Optimization algorithms are often coupled with finite element analysis code in the pre- and post-processing steps. This thesis couples the ANSYS finite element code with an optimization algorithm. In the following discussion, a review of recent research is given in which a similar approach was taken.

A common problem with coupling a finite element code with an optimization method is related to defining the mesh as the shape changes. In general, the definition of a finite element mesh is a manual process that depends on an analyst's past experience, knowledge and intuition (32). It is difficult to automate this procedure when the geometry changes. Nevertheless, this approach is commonly used for optimization analyses. A general approach that works well when coupled with finite element analysis is hard-kill methods, such as ESO methods. They work by gradually removing a finite amount of material from the design domain (26). Bendsoe (33) also coupled finite element analysis and performed shape optimization using the solid/void approach as previously described. The main goal was to replace the discrete nature of the approach and introduce the density as a continuous design variable. Zhou (27) solved a simple truss layout problem for compliance using an iterative continuum-based optimality criteria (COC) method. A finite element program was combined with an optimization algorithm as well. Bendsoe's work was further developed by Suzuki

(34) who coupled a finite element code with an algorithm for shape and topology optimization. They were able to find a numerical solution comparable with an analytical solution for a Michell truss shape. A shape and topology optimization was conducted for multiple loading scenarios as well. Another problem that frequently occurs when finite element analysis is coupled with topology optimization is that the finite element model experiences numerical singularities that do not exist in the physical model. This problem was addressed by Jog (35). He suggested several strategies to stabilize solutions such as using filters in post-processing operations.

4.3 Heuristic Approaches to Optimization

Optimization techniques can be broadly classified as either continuous or heuristic techniques. For continuous functions, there are zeroth-order, first-order and second-order information that are used by different techniques to find the optimum solution. Some common approaches are the Golden section method, Powell's method of conjugate direction, BFGS, and the Augmented Lagrangian Method. These methods are derived from a common principle in which the search direction at a starting point is determined by evaluating the objective function so that it has a lower value and it travels the maximum amount in that direction. This process is repeated until an optimum is reached. Note that this set of problems can also incorporate multiple constraints.

Heuristic approaches are more suitable for black-box optimization. Some common optimization techniques are Simulated Annealing, Genetic Algorithms, and Particle Swarm Optimization. In these techniques the function is not continuous and so there may not be a

clear pattern between the objective function at one point as compared to another. Heuristic approaches try to refine the selected points based on information from a previous set of results. These methods can accept discrete and continuous variables. One distinct characteristic of heuristic approaches is that it is not known if the global optimum has been reached. In addition, different simulations using the same algorithm may often yield different results.

Genetic Algorithms use random number generation to find specific values for the design variables and it progresses towards a solution without regard to how the function is evaluated (36). The algorithm gets its name because of the similarity to genetics. A set of designs is developed from random numbers which constitute the initial generation. Based on the function values the fittest designs are selected, and are used to create 'children' or new designs for a subsequent generation. Every generation also has some 'mutated' designs or randomly generated designs. This approach is extremely flexible and is widely used in many engineering disciplines for finding an optimum solution.

Another heuristic method is called Particle Swarm Optimization. This method is similar to genetic algorithms in the fact that the initial set of designs is generated from random numbers (37). Once the objective function is evaluated, a particular design or 'particle' remembers its coordinates in hyperspace. Each particle has a position and velocity. The position and velocity of a given particle are dependent on the objective function value at the current position as well as the objective function value of other particles at their respective positions. The velocity and position determine the next point of evaluation for a

particle. In this manner, all particles move around the hyperspace and find the best fitness (36).

Another popular heuristic method is called Simulated Annealing. Like its name, the algorithm is inspired by the annealing process. A space might have multiple local minima and if a design solution is stuck in such a local minimum, an algorithm must be able to accept objective function values of greater value before descending to the global minimum. A random point is evaluated initially. Then, a second point is evaluated and the objective functions are compared. If the objective function is less, the new coordinates are accepted and the objective function value is updated. If the objective function of the new point is higher, then the new point is sometimes accepted and sometimes rejected. The acceptance is dependent on the probability density function (PDF) of the Boltzmann distribution. If the density is greater than a random value generated, the point is accepted. Otherwise, the algorithm reverts to the previous point. As the number of iterations increases, the PDF decreases and fewer unsatisfactory points are accepted (36).

This completes the review of the optimization concepts used in the thesis. In the following chapters, these concepts are applied to a specific problem to achieve an optimum design.

5. PROBLEM DESCRIPTION

5.1 Overview of the Thesis

In the previous chapters, a review of the additive manufacturing (AM) industry was described, and the concepts of a Michell truss layout and topology optimization were discussed. As described in the Introduction, a technique to determine the topology of a part is developed in this thesis. The topology is inspired by a Michell truss layout and optimized using an existing heuristic technique. Srithongchai created a design of a simply-supported beam that was inspired by a Michell truss layout (28). A part was manufactured with a CNC milling machine and several tests of the truss were conducted. This paper and its results are presented in the following section and it forms the basis for this thesis. The results from Srithongchai (28) are subsequently used to validate the technique developed in this thesis.

5.2 Summary of 'A theoretical and experimental investigation of a family of minimum-weight simply-supported beams' (28)

A summary of the paper 'A theoretical and experimental investigation of a family of minimum-weight simply-supported beams,' authored by Sriruk Srithongchai, Murat Demircubuk, and Peter Dewhurst is presented in this section (28). The Michell truss layout described in this paper is used as a basis for demonstrating the optimization technique developed in this thesis. The authors used a matrix method to find a solution for a simply-supported beam topology and the reaction forces. A CNC milled aluminum alloy plate was

tested and deflections were compared with theoretical results. The subject is a symmetrical beam case study as shown in Figure 5.1.

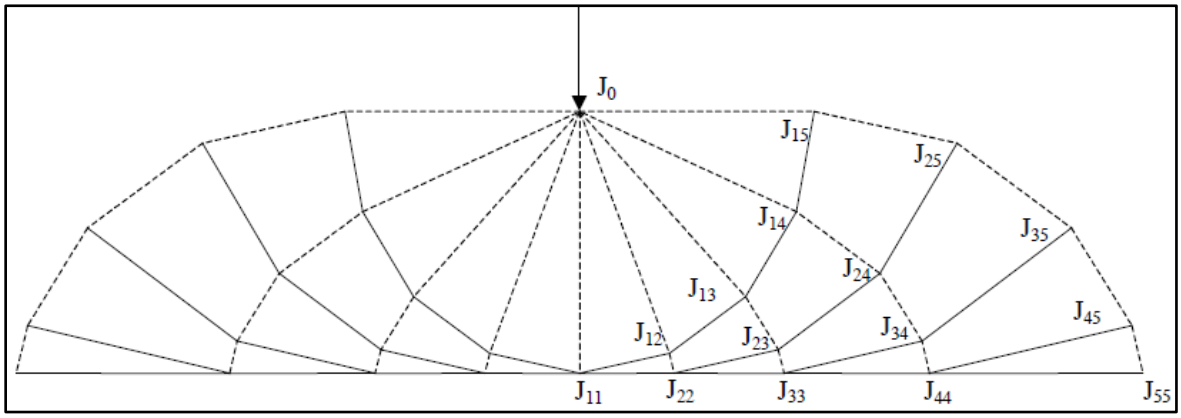

Figure 5.1 Symmetrical Simply-Supported Beam (28)

The joint coordinates are shown below in Table 5.1. Note that these numbers are rounded off to the nearest hundredth. The dimensions are based on a height of unit length and so they may be scaled accordingly.

Table 5.1: Unit Joint Coordinates (28)

J0	J11	J12	J13	J14	J15	J22	J23
(0,1)	(0,0)	(0.38,0.08)	(0.71,0.29)	(0.92,0.61)	(1,1)	(0.4,0)	(0.85,0.09)
J24	J25	J33	J34	J35	J44	J45	J55
(1.28,0.38)	(1.61,0.88)	(0.87,0)	(1.46,0.12)	(2.10,0.56)	(1.49,0)	(2.35,0.18)	(2.4,0)

For a unit load applied at the location shown above in Figure 5.1, the reaction forces in each of the tension and compression members to the left of the joint are shown in Table 5.2. These numbers are also rounded to the nearest hundredth and will be used to validate of the beam model in Section 5.5.

Table 5.2 Reaction Forces for Unit Load (28)

J0	J11	J12	J13	J14	J15
-	(0,-0.08)	(0.22,-0.16)	(0.21,-0.27)	(0.18,-0.31)	(0.13,-0.67)
J22	J23	J24	J25	J33	J34
(0.98,-0.08)	(0.37,-0.19)	(0.32,-0.25)	(0.25,-0.65)	(0.60,-0.05)	(0.26,-0.14)
J35	J44	J45	J55		
(0.23,-0.60)	(0.33,-0.04)	(0.19,-0.56)	(0.13,-0.52)		

As described previously, the beam was machined with a CNC mill and the cross section is similar to the one shown in Figure 5.1. A photograph of this beam is shown in Figure 5.2. The depth is 25mm, the span of the entire beam is 350 mm, and the volume is 275 cm^3. The beam was made of 6061 T6 Aluminum which has a yield strength of 276 MPa.

Tests conducted on this beam which was balanced on the two ends in order to restrain the downward movement. A force was applied in the downward direction at the center. A maximum stress of 260 MPa was assumed before yielding. It was calculated that in the elastic region, a 38.76 KN force is needed for a millimeter of deflection (28). The paper

reports the overall volume of the optimized truss, but no specific thickness for each strut in the truss is provided.

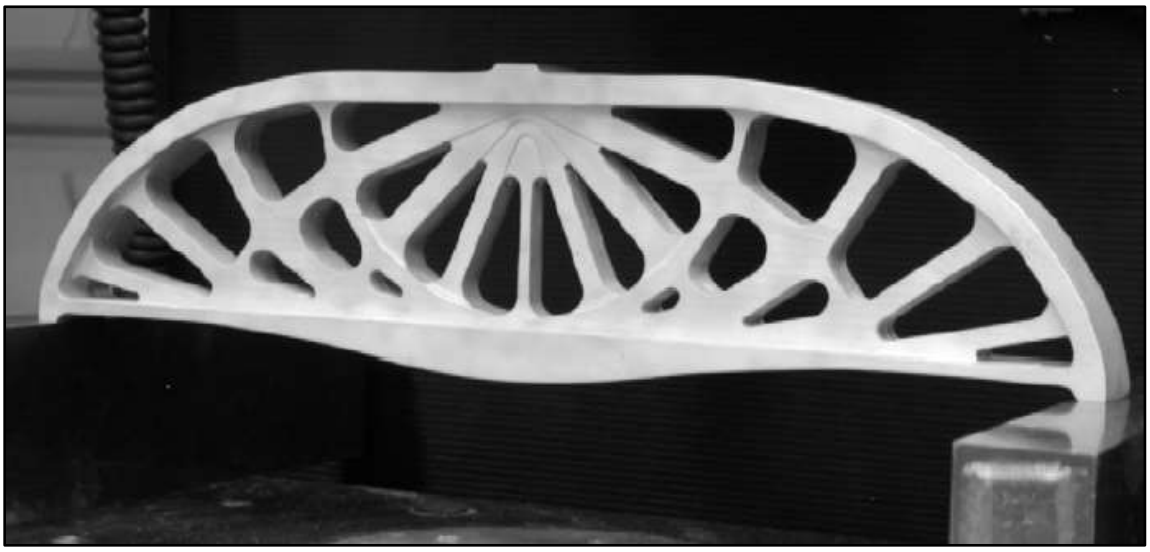

Figure 5.2 Image of Symmetrical Simply-Supported beam (28)

Reference (28) provides two important graphs to describe the properties of the simply-supported beam. Figure 5.3 shows the strain as a function of the stress applied. This graph shows non-linear behavior near and after 276 MPa which is the yield strength of the material. The slope of the linear region is used to calculate the elastic modulus as 74265 MPa.

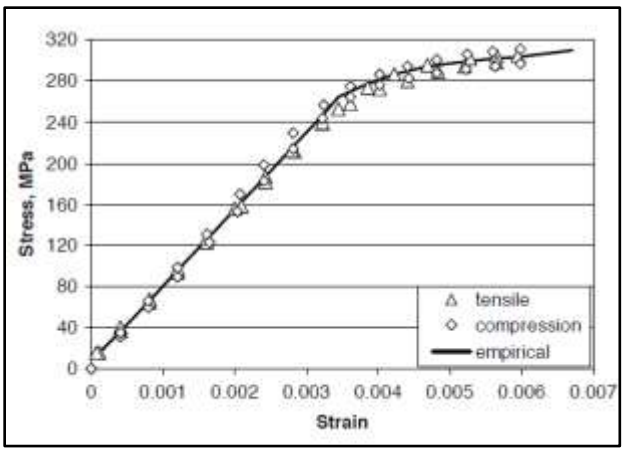

Figure 5.3 Stress-Strain Curve of Simply-Supported Beam

The deflection is shown in Figure 5.4. The maximum deflection occurs close to the bottom left of the beam and it is experimentally calculated. The experimental results were obtained through a load test. The deflection was calculated for different loads. For a load of 98.5KN a deflection of 2.54 mm was expected. This was considered the maximum load before non-linear behavior occurred. The test was halted at the onset of buckling.

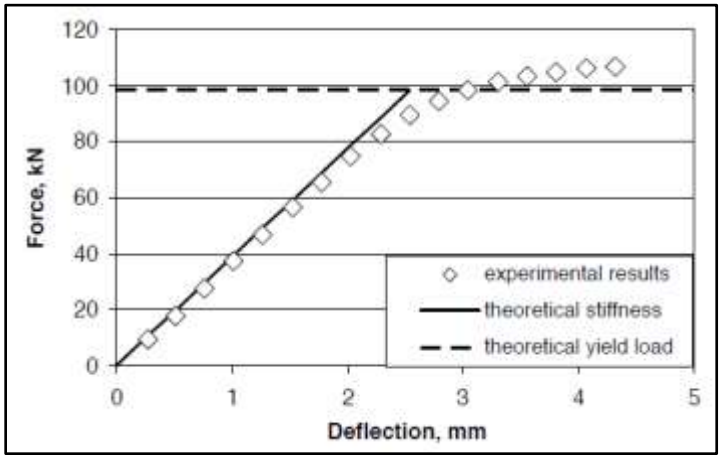

Figure 5.4 Force-Deflection Curve for Simply-Supported Beam

In the following chapters, the optimum design of a Michell truss is found using the optimization technique developed in this thesis. The optimum design is validated using the results of Reference (28).

5.3 FEA Model of a Simply-Supported Beam

For the model described Reference (28), a finite element model of the symmetrical simply-supported beam was created. The objective is to couple an optimization algorithm with the FE model in the pre- and post-processing stage so that the mass of the beam can be minimized. The ANSYS APDL software was used since it is a widely accepted industry standard FE code. In the following section, the ANSYS model is explained in detail. The details of coupling it with an optimization algorithm are discussed in Chapter 7.

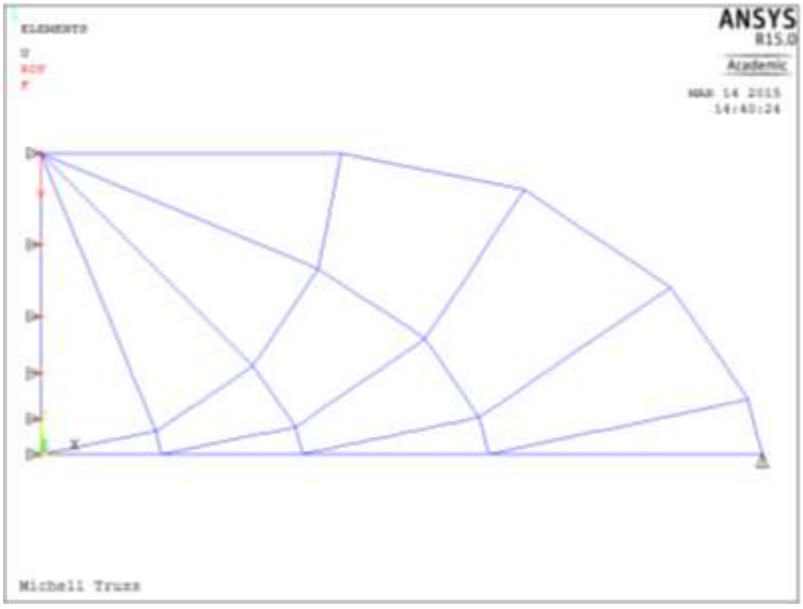

Figure 5.5 Simply-Supported Beam Model in ANSYS APDL

The simply-supported beam is modeled as a linear elastic material using BEAM3 elements. The ANSYS model is shown in Figure 5.5. Half the beam is modelled and a symmetric boundary condition is applied on the other half. The force applied is halved to account for this symmetry. The Keypoints are defined at locations as described in Reference (28) as shown in Table 5.1. For each unit length of 1, an equivalent distance of 72.91 mm was taken in accordance with the dimensions listed in Reference (28). For the ANSYS model, half-span of the beam is 175 mm. The Keypoints are connected by lines.

5.4 Boundary Conditions

Figure 5.2 shows constraints on the bottom right and left ends of the symmetrical simply-supported beam which prevent it from moving down. This is modelled by applying a constraint on the bottom right keypoint and preventing it from moving in the vertically. To account for symmetry, the line on the left is not allowed to move horizontally. A downward force is applied at the top left keypoint. A force of half the magnitude is applied to account for the symmetry condition.

The ANSYS model is coupled with and controlled by an optimization algorithm. The boundary conditions as well as other model parameters such as the depth, location of the keypoints and the lines connecting these keypoints are held constant. The input for the ANSYS model is defined in a text file. For a given design, the only variable in the model is the thickness of each of the lines. The optimization algorithm will be used to determine the optimal thickness of each of the lines. The moment of inertia and the cross section of each line are dependent on thickness and so they vary as the thickness values change. In the next

section the results for this ANSYS model as well as other post-processing steps are described.

5.5 Validation of the Beam Model

The model was validated by comparing the internal forces of each of the members with the published forces in Reference (28). The boundary conditions described in the previous section were applied and a force of 0.5 N (half of a unit load to account for symmetry) was used. The areas and thicknesses were set to unity as well. The line numbers that will be used for comparison with Reference (28) are shown in Figure 5.6. The model was then solved to determine the optimal member thicknesses.

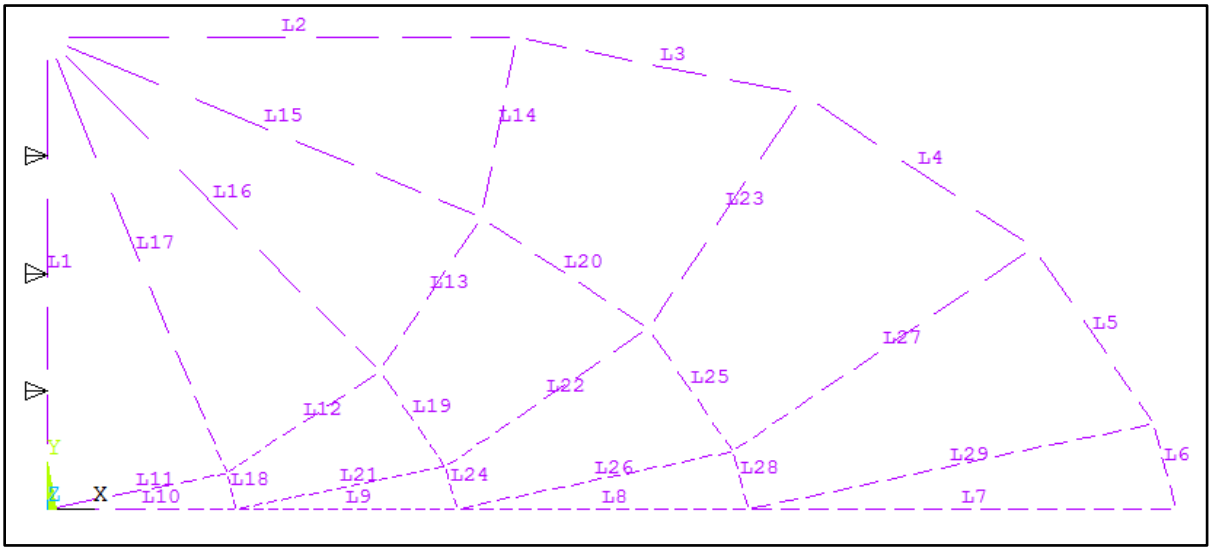

Figure 5.6 Line Numbers for Reaction Force Comparison

Once the model was solved, the axial stress values across the model were obtained. The axial stress shown in Table 5.3 is constant along a line.

Table 5.3 Comparison of Internal Forces for ANSYS Model and Published Results (28)

Line No.	ANSYS value for Force	Paper ref (28)	Published Value (28)
1	-0.0438	J11c	-0.0875
2	-0.66613	J15c	-0.666
3	-0.65333	J25c	-0.6532
4	-0.60473	J35c	-0.6046
5	-0.55943	J45c	-0.5594
6	-0.51705	J55c	-0.5169
7	0.1317	J55t	0.1321
8	0.32729	J44t	0.3275
9	0.59653	J33t	0.5965
10	0.98102	J22t	0.981
11	0.22429	J12t	0.2243
12	0.21396	J13t	0.2139
13	0.17873	J14t	0.1786
14	0.13016	J15t	0.1301
15	-0.30714	J14c	-0.3072
16	-0.26752	J13c	-0.2676
17	-0.16187	J12c	-0.1618
18	-0.077	J22c	-0.077
19	-0.19409	J23c	-0.1941
20	-0.2514	J24c	-0.2515
21	0.37217	J23t	0.3722
22	0.32336	J24t	0.3253
23	0.24712	J25t	0.2472
24	-0.0549	J33c	-0.0548
25	-0.13756	J34c	-0.1377
26	0.26065	J34t	0.2604
27	0.22645	J35t	0.2261
28	-0.0404	J44c	-0.0406
29	0.18937	J45t	0.19

For the joints shown in Table 5.3, a subscript ‘c’ denotes a compression member to the left of the joint as shown by the dotted line in Figure 5.2. The subscript ‘*t*’ is used to denote a member in tension as shown by a solid line in the same figure. The internal forces in the numerical model show excellent agreement with the published results except for the first line. This value is exactly half because the numerical model represents half the value of the actual thickness of the line. Hence, it can be concluded that the ANSYS numerical model is similar to the model described in Reference (28).

5.6 Post Processing of the Finite Element Model

The model described in the previous section was used to compute the following results. For a constant thickness value of 10 mm for all struts of the beam, the deformed shape is shown in Figure 5.7.

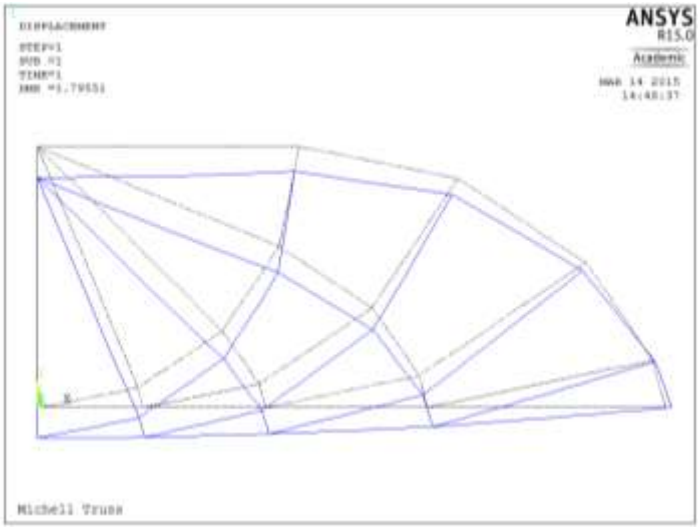

Figure 5.7 Deformed Shape of Simply-Supported Beam Model (blue)

The blue solid lines represent the deformed shape and the black line is the un-deformed shape. As expected, the left side of the beam model deforms in the negative y-direction because of the force applied at the top left corner in the downward direction. The maximum deflection for this model is 1.93 mm. Note that the deflection for the constant thickness of 10 mm are expected to be stiffer than the tested model. Since the beam is represented by beam elements, some of the struts might have overlapping material.

The outputs of interest are the maximum and minimum stress of each strut. The maximum stress is found by adding the axial and bending stresses and the minimum stress is found by adding the two stresses as if they were compressive. Figure 5.8 shows the maximum stress throughout the model. It is important to note that the stress numbers that exceed the yield stress limit are inaccurate because the model is based on the assumption that the material is linear elastic. Therefore, the only valid conclusion is that the stresses exceed the yield strength.

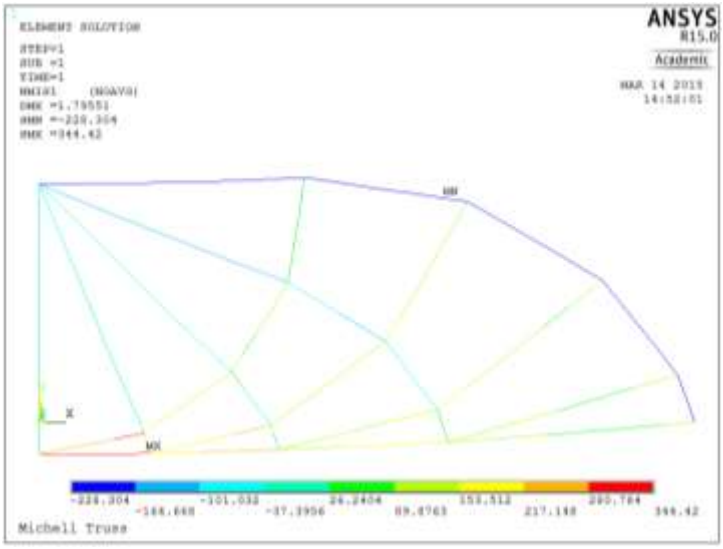

Figure 5.8 Maximum Stress in Simply-Supported Beam Model

As expected, the alpha lines are in tension and have tensile stresses. Some struts in the beam are stressed above the yield limit as well. The element stresses are stored in a text file and read back to MATLAB for each design evaluation in the optimization algorithm. The initial thickness value of 10 mm is not optimized.

5.7 Summary

The Srithongchai paper (28) was reviewed and a finite element model of a simply-supported beam was described. The deformed shape and maximum stress value was found for a constant thickness of 10 mm for all struts. Note that the struts are represented by lines for which the cross sectional area and moment of inertia are defined. The beam model was validated by comparing the internal forces with the published values in Table 5.2. In the next chapter, an approach for the derivation of internal slip lines in a beam is introduced.

6. GENERAL STRUCTURAL LAYOUT OF A MICHELL TRUSS

6.1 Principal Stress Trajectories for a Simply-Supported Beam

To find the optimum topology for a given design, the layout of the Michell truss is first determined by describing the location and direction of the slip lines throughout the field. As described in Chapter Two, the slip lines represent the directions of the principal stresses throughout the field. However, the slip line trajectories are tedious to find. Melchers (38) recently described extending the range of Michell-like optimal topology structures by showing slip line layouts for different loading conditions. To define complex equations, numerical and analytical methods have been developed to find the slip lines for relatively well-defined problems such as a simply-supported beam and a cantilever beam. The Matrix method (39) and the Ewing Power Series (23) method are two such examples. These techniques result in complex equations and a simpler method is needed to define the layout of a Michell truss.

In a recent paper on optimum structural design, Barnett found that the members in an optimum structure must lie along the lines of principal strain. Otherwise, a direction could be found at a point on a member for which the direct strain had a magnitude greater than the current strain (40). Timoshenko (41) also discusses the trajectories of principal stress for plane stress applications. The trajectories of the principal stresses for a simply-supported beam with uniform loading are shown in Figure 6.1. Note that the trajectories coincide with the direction of the principal stress at a given point. The magnitude of the principal stress is not uniform along the trajectory lines.

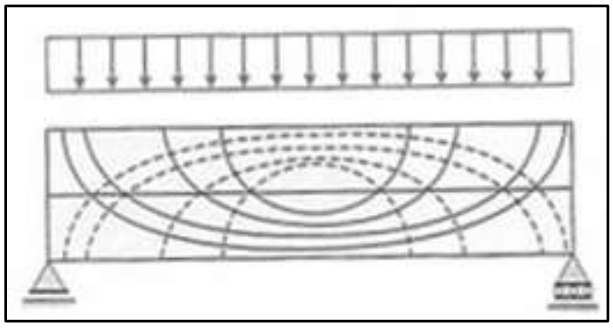

Figure 6.1 Principal Stress Trajectories for a Simply-Supported Beam (41)

6.2 Principal Stress Trajectories using Finite Element Analysis

As discussed in the previous section, it is known that the principal stress trajectories for a given loading condition coincide with the direction of the slip lines. The topology of the model and the exact placement of material is the central objective for optimization. These slip lines which define the position of material can also be derived by creating a finite element model of the outside periphery of the design. Once the principal stress trajectories are obtained from such an analysis, the slip lines can be constructed to create the internal geometry of the lattice structure. The simply-supported beam described in Chapter 5 is used in this thesis to demonstrate this correlation. The Michell truss in Reference (28) is also used to demonstrate the correlation.

6.3 CAD Model and FEA Model

A Computer Aided Design (CAD) model of the simply-supported beam was created in SolidWorks using the dimensions described in Chapter 5. The outer boundary of the beam was modeled while the interior region of the beam was treated as a complete solid.

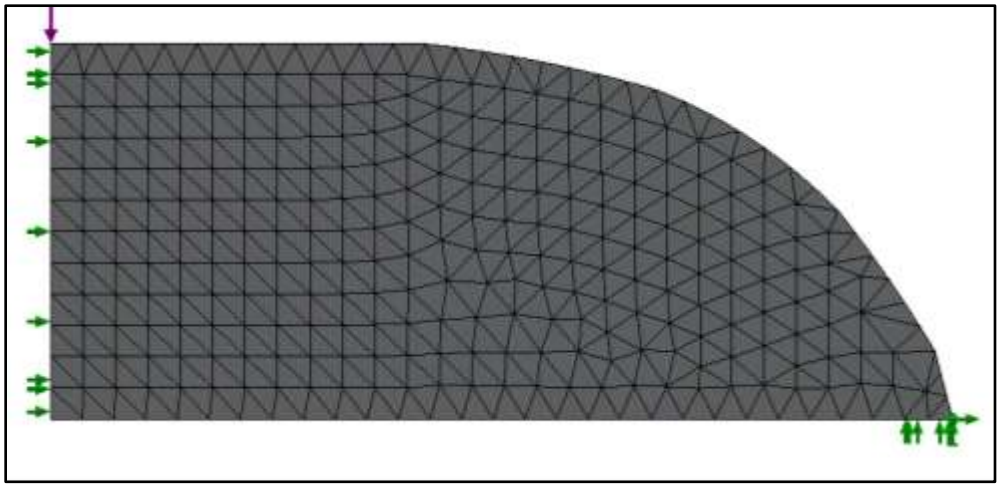

Figure 6.2 Finite Element Model Showing Constraints and Loads for Simply-Supported Beam

Figure 6.2 shows the overall geometry of the beam. Only half of the beam is modeled and a symmetry condition is used along the left edge. The right bottom point is fixed in the vertical direction representing a constraint on the model. The left top most point is the location of the force. To account for symmetry the left-most edge is not allowed to move horizontally. The model is defined as two-dimensional plane stress and triangular elements

are used. The material is aluminum 6061 T6 which has a yield strength of 276 MPa, an elastic modulus of 6.9e4 N/mm^2, and a Poisson ratio of 0.33.

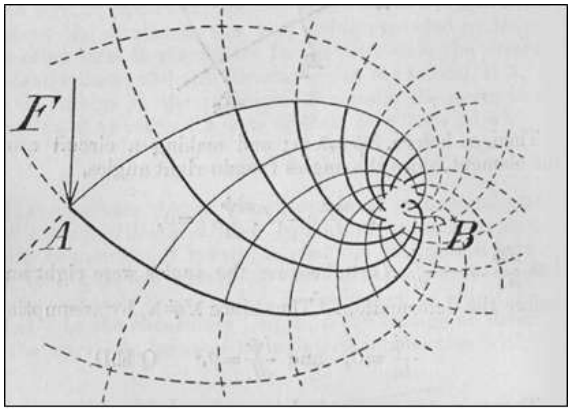

Figure 6.3 Original Michell Paper Example (3)

For a cantilever beam, the initial shape of the Michell truss is shown in Figure 6.3 (28). The force is applied at point A and point B is fixed. Figure 6.4 shows the geometry as setup in SolidWorks Simulation. A force is applied on the left and the right face is fixed. Triangular elements are used and the material is aluminum. The results for this model are discussed in the next section.

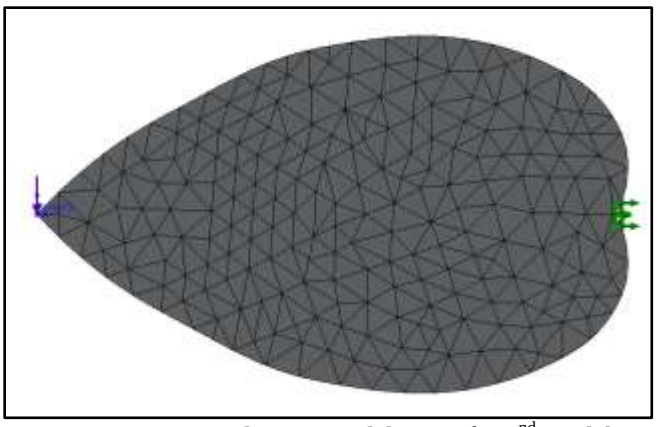

Figure 6.4 Finite Element Model Setup for 2nd Model

6.4 Plane Stress Model Results and Discussion

The principal stress trajectories for this finite element model are shown in Figure 6.5. Based on the initial shape as described by the experimental results, a separate Michell truss CAD model was created and this is superimposed in this figure. Note that the trajectories align with the direction of the Michell truss struts and the slip lines. As shown, the principal stress trajectories align with the alpha and beta lines of the internal lattice structure of the model in Reference (28). There are large stresses near the support which is indicated with a large arrow. These large stresses are ignored in this analysis. Note that the lines and directions are also dependent on the density of the finite element mesh.

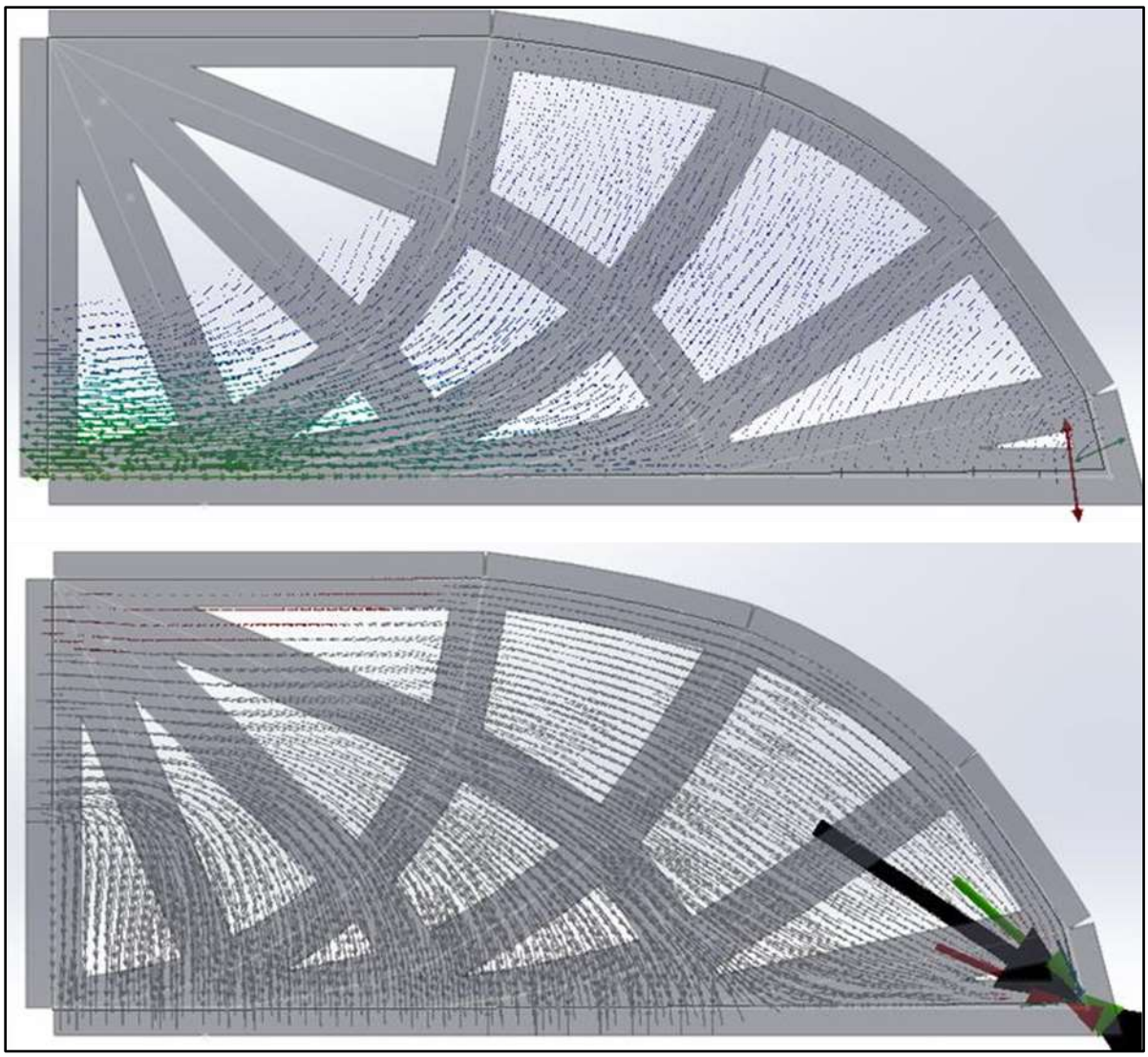

Figure 6.5 Maximum and Minimum Principal Stress Trajectories Superimposed on the CAD Model

The stress trajectories for the beam described in Michell 1904 (3) paper is shown in Figure 6.6. The slip lines in Reference (3) align with the principal stress trajectories as found from the plane stress finite element model.

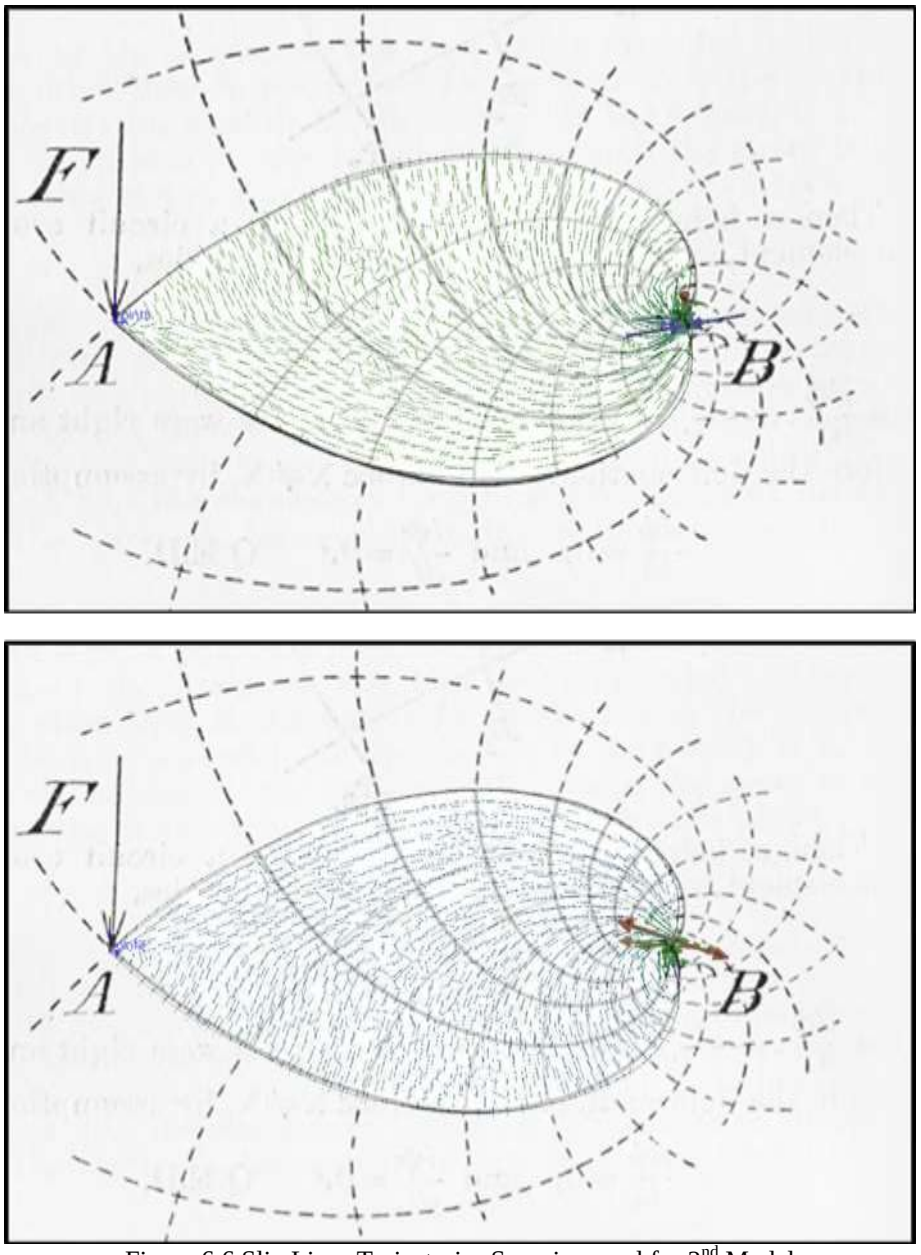

Figure 6.6 Slip Lines Trajectories Superimposed for 2nd Model

As shown in the previous results, the principal stress trajectories are a positive indication of the placement of struts on the interior of the beam. This method does not describe how many internal lines should be used; that is solely dependent on the designer and

manufacturing limitations. The thickness of each of the line is also unknown. This results in the stiffest structure for a given mass. As explained in Chapter 2, Michell trusses have certain limitation. The yield strength in compression and tension must be the same and plane stress conditions must be satisfied. These assumptions are adhered to when creating the finite element model used in the above examples.

Since the stress along each line can change, an optimization algorithm is needed to find the appropriate thickness for each slip line. The next chapter describes the optimization algorithm as coupled with a finite element model.

7. OPTIMIZATION ALGORITHM

7.1 Introduction

In Chapter 4, several common topology optimization techniques were reviewed. In this thesis, a Michell truss is assumed to represent an optimum layout of a lattice structure. This initial shape is found using directions of the principal stresses trajectories. It is important to note that the stresses are not uniform along the principal stress trajectories. The stress values are also dependent on the thickness and area of each strut in the lattice. The mass is also dependent on the area of each strut. A heuristic technique called simulated annealing is used to find the thickness of each strut in the lattice so that the mass is minimized. In this chapter, the optimization problem is formulated and the parameters used in the algorithm are described.

7.2 Method Formulation of the Optimization Problem

The objective of the optimization problem is to minimize the mass without violating any of the constraints. One such constraint is that the maximum allowable stress for all struts of the beam be less than the yield strength (σ_y). ANSYS was used to calculate stress. A description of the ANSYS model was provided in Chapter 5. The thicknesses of each strut in the lattice constitute the design variables of the optimization problem. The optimization problem in standard form is as follows:

Minimize: $Mass = \rho * depth * \sum(length\ (i) * thickness\ (i))$

Subject to: $Stress\ value\ (i) - \sigma_y <= 0$

$Thickness\ (i) > 0$

Where 'i' represents the number of design variables and is equal to the number of struts in the ANSYS model. The simply-supported ANSYS beam model has 29 struts. The length of all lines is constant and static during the optimization. In Chapter 4, various methods commonly employed for topology optimization were described. In this thesis, the optimization algorithm is coupled with a finite element model.

7. 3 Method: Description of the Algorithm

To optimize the thickness of each strut a simulated annealing optimization algorithm was developed using MATLAB and then coupled with the ANSYS finite element analysis software. There are 29 lines in the ANSYS model and a uniform thickness is assumed along each line. Hence, there are 29 thickness values to be determined using the optimization algorithm. Figure 7.1 shows a flowchart that describes the steps in the algorithm.

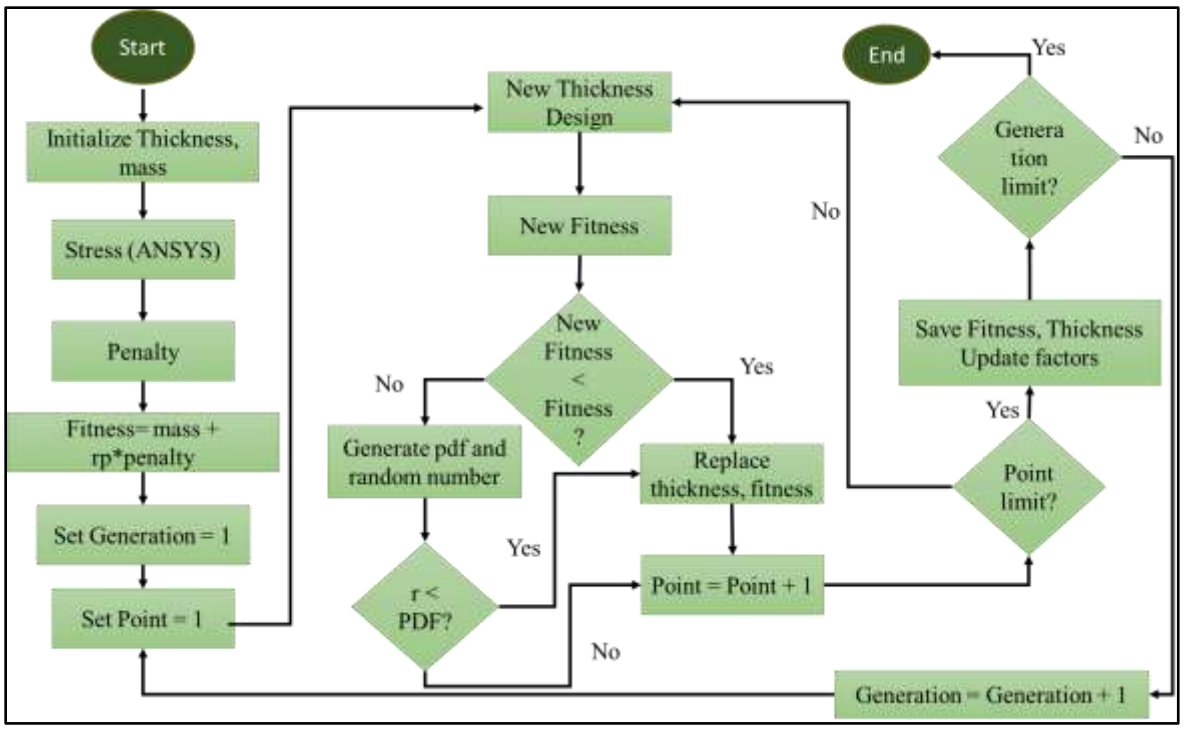

Figure 7.1 Flowchart for Simulated Annealing Algorithm

An initial design of thickness values for all of the struts is entered. This initial design is a constant thickness value of 5, 10, or 15 mm for all struts. Based on the length, depth and density of each strut, the volume and mass of a current design can be calculated. The stress values for the constraints are calculated in ANSYS as described earlier and read back into MATLAB. The maximum and minimum stresses are determined and the absolute value is found. Then, the maximum values of these two stresses are established. The difference of any stress value and the yield strength is added as a penalty if it is above the yield strength. This penalty is multiplied by an '*rp*' factor. The overall objective of the algorithm is to minimize the fitness. The fitness of a given design is defined as

$$Fitness = Mass + Penalty * rp$$

The penalty and mass calculations are defined above. The '*rp*' value changes as the algorithm progresses and it will be explained in the following discussion.

7.4 Generating a New Design

Once the initial fitness is calculated, the counter for the number of iterations and design evaluations per iteration begins. A new design is generated and the fitness values are compared. To generate a new design a varied approach is used. If there are stress violations (and subsequently penalty) in the previous fittest design held, a new design is created by randomly selecting ten thickness values and perturbing it. For a selected thickness value, if the corresponding stress in that strut in the previous design is above the yield strength, the new thickness will increase in value between 0 and 1 of the previously held value.

$$new\ thicknessvalue(i) = thicknessvalue(i) + rand$$

Where '*rand*' is a random number between 0 and 1. For the selected thickness, if the corresponding stress is below the yield strength, the new thickness can be perturbed upwards or downwards.

$$new\ thicknessvalue(i) = thicknessvalue(i) - 0.5 + rand$$

The thickness is allowed to increase or decrease because the stress values of all struts are coupled. Hence, if the thickness of a particular strut decreases, its corresponding stress

may still be below the yield strength, but the stress of an adjoining strut might increase above the allowable limit.

If all stress values are below yield for the previous fittest design, a different approach for design creation is used. Only one thickness value is selected out of 29 and it is changed as follows:

$$new\ thicknessvalue(i) = thicknessvalue(i) - 0.7 + rand$$

Since the stress values of all struts are below yield, the selected member has a higher probability of decreasing in value based on the above equation. This approach was selected based on parameters from research on topology optimization using simulated annealing (42).

7.5 Accepting a New Design

Once a new fitness is calculated based on the new design described above, it is compared to the existing fittest design. If the fitness of the new design is lower, it replaces the existing design as the new fittest design and its thickness values are stored.

If the new design does not have a lower fitness, its acceptance is dependent on a probability density function (PDF). This value 'p' is determined by the following equation:

$$p = e^{\frac{delta\_e}{t}}$$

Where $delta_e = fitness - new\ fitness$

t is the temperature at each iteration

'*delta_e*' is a negative value when the new fitness is higher than the existing fittest design. The value of '*p*' is always between 0 and 1 when calculated as described above. This value is compared to a random number generated by Matlab between 0 and 1. If '*p*' is higher, the bad design replaces the current fittest design; and if '*p*' is lower, the algorithm continues with the previously held fittest design. The process of accepting bad designs with higher fitness values allows the algorithm to escape local minimums.

7.6 Cooling Schedule

The temperature '*t*' for a given iteration determines the value of '*p*' and subsequently the probability of accepting a bad design. As the number of iterations increase, the probability of accepting bad designs decreases. The temperature is initially set to 60 and decreases by a factor of 0.990. Hence, for all designs evaluated at a given iteration, the probability of accepting bad designs is held constant. Then, as the iteration number increases, the temperature decreases. The probability of accepting a bad design for the next set of design evaluations will decrease.

In this chapter, the optimization problem was presented and the procedure of the simulated annealing algorithm was described. The objective of the algorithm is to reduce the fitness or minimize mass with constraints being accounted for by using a penalty function. In the following chapter, additive manufacturing constraints are discussed and how they are also incorporated in the optimization algorithm is described.

8. CONSTRAINTS FOR ADDITIVE MANUFACTURING

8.1 Introduction

In the previous chapter, an optimization algorithm was described for determining the thickness for each strut in the symmetrical simply-supported beam. In this chapter, constraints for additive manufacturing (AM) will be explained followed by the method for incorporating these constraints into the algorithm.

Additive manufacturing gives a designer the freedom to design and manufacture complex parts with higher stiffness and less mass as compared with parts that are made with traditional manufacturing processes. As discussed in Chapter 2, additively manufactured parts are successfully replacing multiple components in an assembly and transferring loads within a structure with greater efficiency.

Constraints for additive manufactured parts are highly dependent on the specific process. These manufacturing constraints need to be taken into account when designing a part. Constraints vary based on the material, machine and processes. The design constraints can also be affected by the use of support material in some machines. It is probable that AM machines, materials and processes will continue to improve over time and this will further reduce manufacturing constraints. There have been optimization algorithms in previous research that investigate minimum member thickness constraints (43). However, there has been no research on methods to incorporate specific AM constraints into the topology optimization process. In this thesis, the algorithm described in Chapter 7 will be modified to include a penalty for AM constraint violations.

8.2 Constraints of Additive Manufacturing

As described in Chapter 2, 3D printing technology consists of multiple processes, machines, and a variety of materials. For each unique combination of these, the manufacturing constraints could be different. The following constraints have been obtained from companies such as *Shapeways*, Solid Concepts, *iMaterialize*, and EOS that provide manufacturing services for 3D printed parts. These manufacturing constraints are conservative because the shipping and handling of these fragile and complex parts after manufacturing must also be considered. Since aluminum was used as the material for the optimization algorithm, a similar material will be used here as well. Aluminum is predominantly made using the DMLS method. Table 8.1 shows the constraints and they are explained below.

Table 8.1 Constraints for 3D printing of Alumide (44)

Minimum wall thickness	1 mm
Minimum details	0.4-0.5mm
Accuracy	0.30%
Maximum size	310 x 310 x 400mm
Clearance	0.5mm
Interlocking	Yes
Minimum angle in z-direction	30 degrees

As shown in this table, the minimum wall thickness for every section in the part is 1mm. The minimum tolerance for a part is 0.4mm. Solid Concepts allows an even lower

tolerance of 0.13mm (0.005in.). There is also a minimum clearance of 0.5mm between two adjacent components in the build chamber.

In addition, there are other guidelines that need to be taken into consideration. For example, it is always preferred to have the inside of the part hollowed out to the smallest possible thickness. For powder on the inside to be removed during post-processing, an escape hole or two is usually needed as well (44) as shown in Figure 8.1.

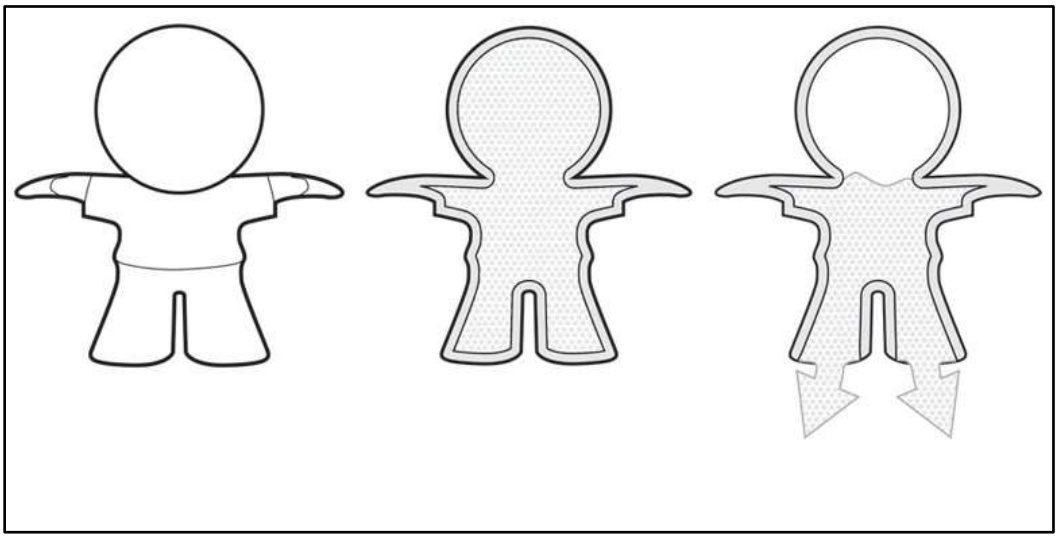

Figure 8.1 Hollow Model with Holes for Powder to Escape (44)

A minimum angle of 35^{o} is recommended by Solid Concepts when not using support material (45). This angle is solely in the direction of the build and not in the x-y plane. In addition to these guidelines, some 3D printing processes have problems with warping and shrinkage that need to be taken into account in advance.

8.3 Incorporating Constraints in the Optimization Algorithm

The AM constraints described in the previous section will be incorporated into the optimization algorithm. There are three specific areas where these manufacturing constraints can be taken into account.

The first area is the initial design. The number of struts is inversely proportional to the thickness of each strut. However, too many struts will cause them to be too close to each other for 3D printing. It is important to know the angle limit as well and the build direction when designing the initial shape. It is assumed that the constant cross section will be in the z-direction for the model to be built. Hence, the angle constraint does not need to be considered when designing the struts for the symmetrical simply-supported beam. The maximum length and breadth of the model should be within the confines of the build volume. The initial design should also take advantage of making complex and hollow parts with strategic placement of holes to remove powder or support material from the interior of the part.

The second area of AM constraint relates to the limits for each thickness design variable. The algorithm randomly determines the design variables (strut thickness) to change, but the range of values are selected by the designer. The minimum wall thickness of 1 mm is used and all design variables are allowed to be assigned a value above this thickness.

The allowable stress values are accounted for by using a penalty approach. All stress values are added and multiplied by an '*rp*' factor. This penalty is added to the mass to find the fitness. The objective of the algorithm is to minimize the fitness or mass. The new equation for fitness is

$$Fitness = mass + rp*penalty + rp\_am*penalty\_am$$

Where the '*rp*' and penalty is for stress violations and '*rp_am'* and '*penalty_am'* are for additive manufacturing constraints.

Any penalty will decrease the chances of a design being accepted as it will have a higher fitness. Similarly, for the minimum clearance between the trusses, the thicknesses at the mid-points are calculated and a penalty is added if it exceeds the minimum 0.5mm limit. For the symmetrical simply-supported beam, the line numbers are shown in Figure 8.2 and the distance between their midpoints is shown in Table 8.2.

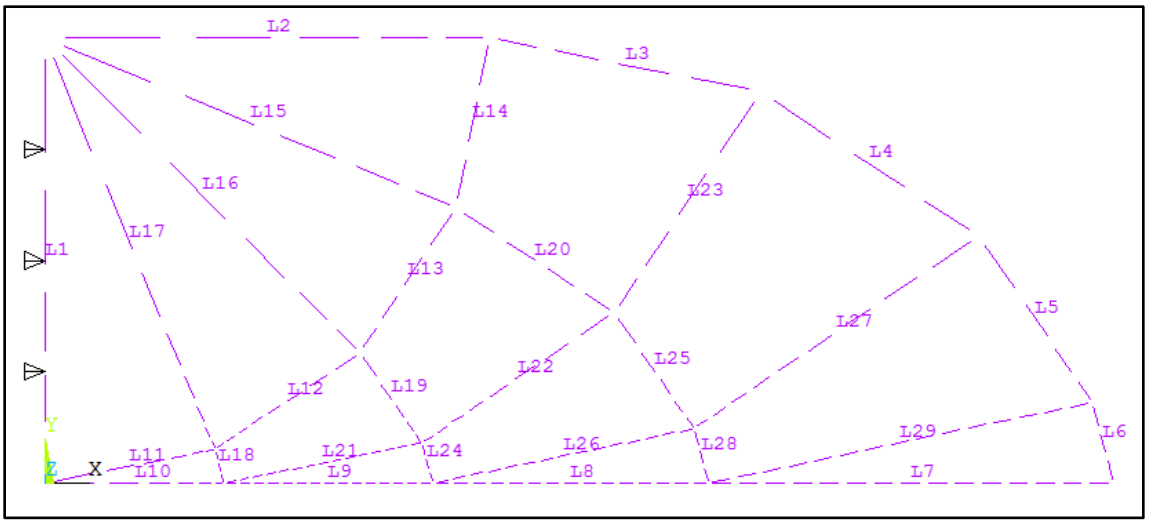

Figure 8.2 Line Numbers for Simply-Supported Beam ANSYS Model

The AM constraints were incorporated into the algorithm for the symmetrical simply-supported beam. All aspects of the optimization algorithm have now been defined. Chapter 5

defined the experimental results based on past research and the finite element model created in ANSYS.

Table 8.2 Distance between Mid-Points for AM Constraints

Alpha Lines	Distance (mm)	Beta Lines	Distance (mm)
L18-L19	32.7	L21-L12	12
L19-L20	35.2	L26-L22	15.73
L20-L3	37.9	L22-L13	26.11
L24-L25	43.4	L29-L27	21.4
L25-L4	54.1	L27-L23	34.5
L5-L28	63.4	L23-L14	41.1

Chapter 6 presented a new method to define slip lines and the internal lattice for a beam design. Chapter 7 defined the algorithm and its formulation for optimization. Finally, this chapter defined the different additive manufacturing constraints for aluminum and described the three specific areas where these constraints can be incorporated.

In the next chapter, the results of the optimization study are described followed by a discussion of a comparison with experimental results.

9. RESULTS AND DISCUSSION

9.1 Background

In the previous chapters, experimental results for a symmetrical simply-supported beam were presented, a new method to find the slip lines for the internal lattice of a design was defined, and an optimization algorithm and its constraints were described. The results of the optimization algorithm are described in this chapter. Additive manufacturing constraints are incorporated in the algorithm and these results are shown separately in a later section of this chapter. The robustness of the algorithm was demonstrated by showing that the minimum weight of the truss was found to be nearly unchanged with different starting points used for the optimization analysis.

9.2 Fitness

For the simply-supported beam, the maximum allowable stress is equal to 276 MPa. A total of 350 iterations were used and 30 designs were examined per iteration. Convergence was assumed when the final design did not change for several consecutive iterations. As described previously, the '*rp*' value increases and the probability of accepting a bad design decreases for further iterations. The mass is calculated in grams and the fitness is the sum of the mass and the penalty times the '*rp*' factor. For the results presented below, the thickness of all struts is initially set to 15 mm.

Figure 9.1 shows the computed fitness of the design as a function of the iterations. Note that the fitness is the sum of mass in grams and the sum of all stresses in MPa above the

yield strength times an '*rp*' factor. The fitness shows good convergence as the number of iterations is increased. The final value of fitness is 560.9g. Since there were no stress violations (no penalty) in the final design, this is also the mass of the final design in grams. The mass is calculated using mass density of aluminum and the lengths of the line model. Note that the truss has overlapping material which is not accounted for in the mass calculations.

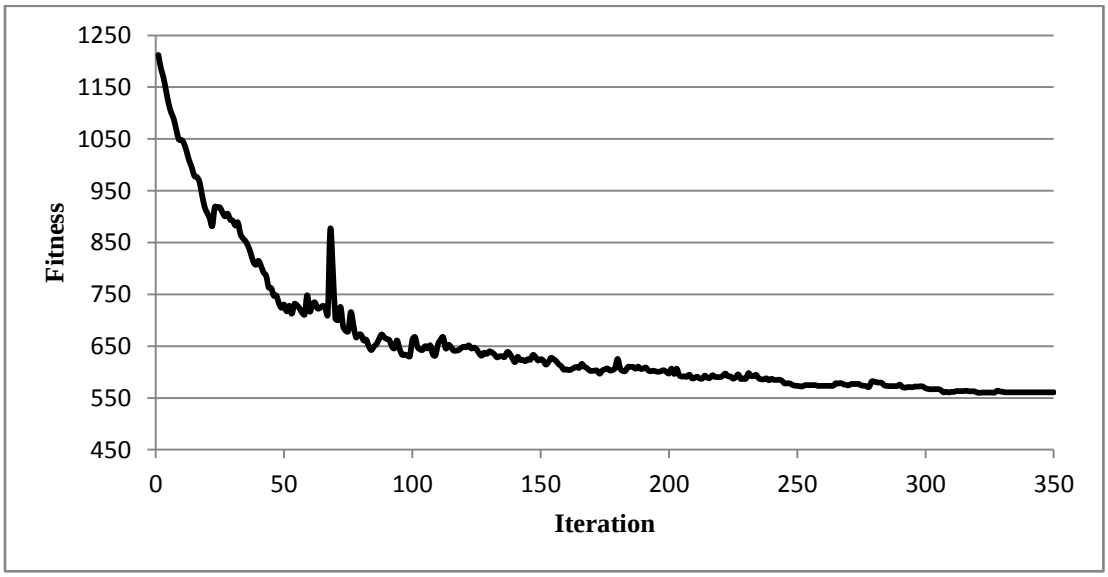

Figure 9.1 Fitness vs Iterations for Symmetrical Simply Beam

9.3 Model Comparison

The optimized strut thicknesses for the minimum weight truss were used to create the CAD model shown in Figure 9.2. Fillets were added to create a smooth transition between

intersecting struts. The mass of the CAD model is 522g. The line model has a higher mass because it assumes a thickness for each line and calculates that mass whereas the CAD model creates an actual three dimensional shape without overlapping material.

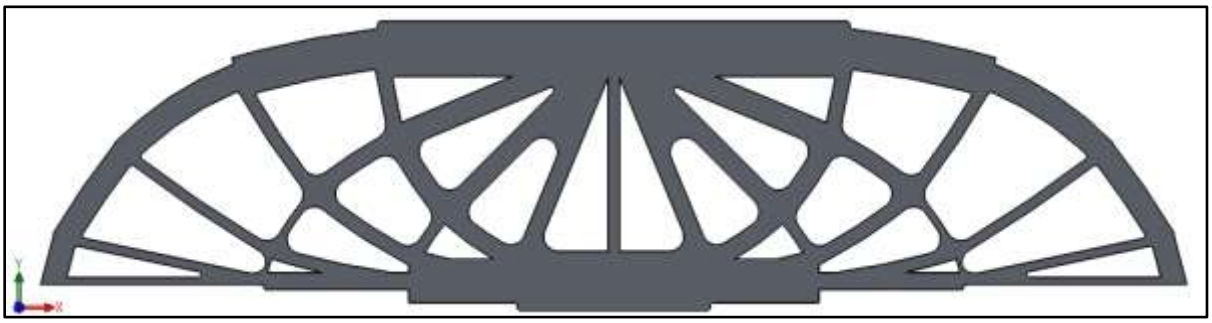

Figure 9.2 CAD Model with Optimized Thicknesses

A visual comparison can be made between the results of this thesis and the reference truss (28) shown in Figure 5.2. Note that the thickness of each strut in the simply supported beam was not provided. In this thesis, it was found that the thicknesses along each alpha and beta line changes gradually and no abrupt changes in thickness occurred. This is consistent with the beam solution in Reference (28). Other similarities can be noted. For example, the center strut for both the reference truss and the optimum beam analyzed in this thesis has a very small thickness. Another similarity between the two is that the horizontal strut at the bottom of the beam is thinnest near the supports and thicker towards the center. Note that the reference beam has a constant thickness for the outside struts, whereas the numerical optimized model has a gradual decrease in thickness. In addition, the optimum beam does not

have any abrupt thickness changes and the thickness along each alpha and beta line changes in a uniform fashion.

9.4 Stress Results

The optimized fitness corresponds to the minimum mass of the beam. The fitness for a given iteration is dependent on the stress values. Note that the optimized fitness is equal to the minimum mass. Figure 9.3 below shows the maximum stress as a function of the iterations. The absolute value of maximum stress exceeds the yield strength of 276 MPa in the initial iterations. However, with further iterations, it varies close to the yield strength and finally settles to a value that does not exceed 276 MPa for the final design.

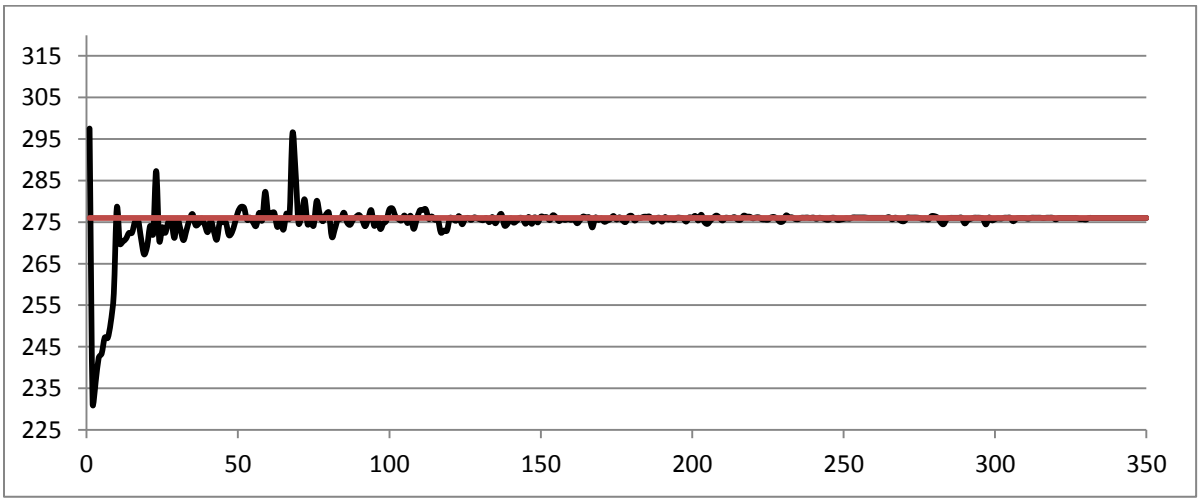

Figure 9.3 Maximum Stress vs Iteration

An ANSYS model of the minimum weight truss was created using the optimized strut thicknesses. The maximum and minimum stresses are of interest. Figure 9.4 shows the distribution of maximum tensile stress which is the sum of axial and bending stresses in the tensile direction of all trusses. Figure 9.5 shows the minimum compressive stress which compressive of the sum of axial and bending stresses in the compressive direction for all trusses. Note that the absolute value of these stresses does not exceed the 276 MPa yield strength of aluminum.

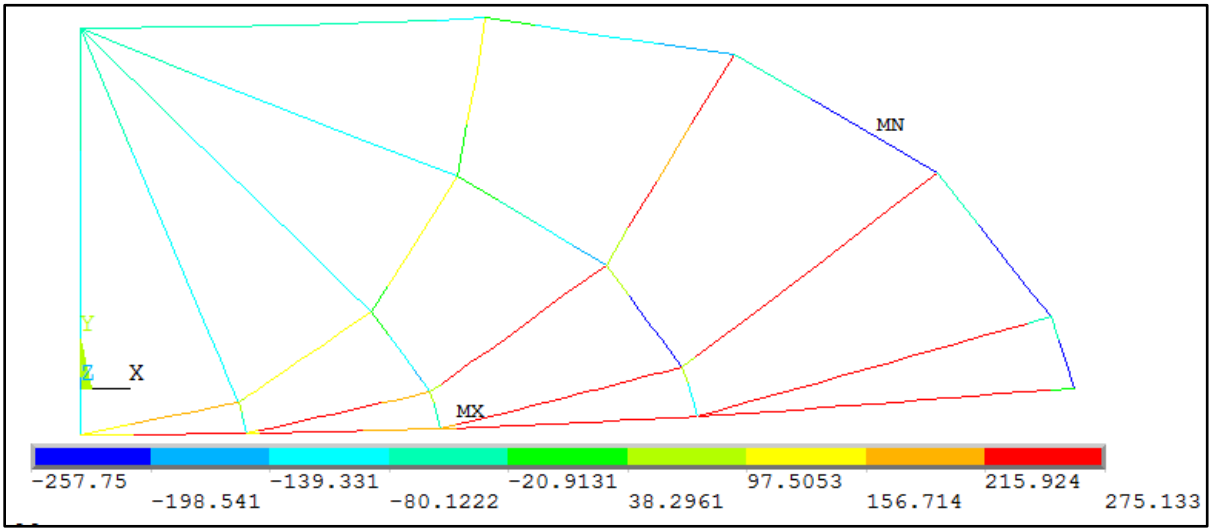

Figure 9.4 Maximum Stress Distribution for Optimized Design

The maximum stress or beta lines are in tension. Four out of the five beta lines are shown in red and one of them is yellow. Since the stress is close to yield, this suggests that

the thickness is sufficient small so that a global optimum has been reached for a particular truss.

The corresponding minimum stress distribution is shown in Figure 9.5. This stress distribution coincides with the compressive alpha lines and the compressive stress limit of -276MPa. The least stress occurs along the top outermost strut which is shown in dark blue.

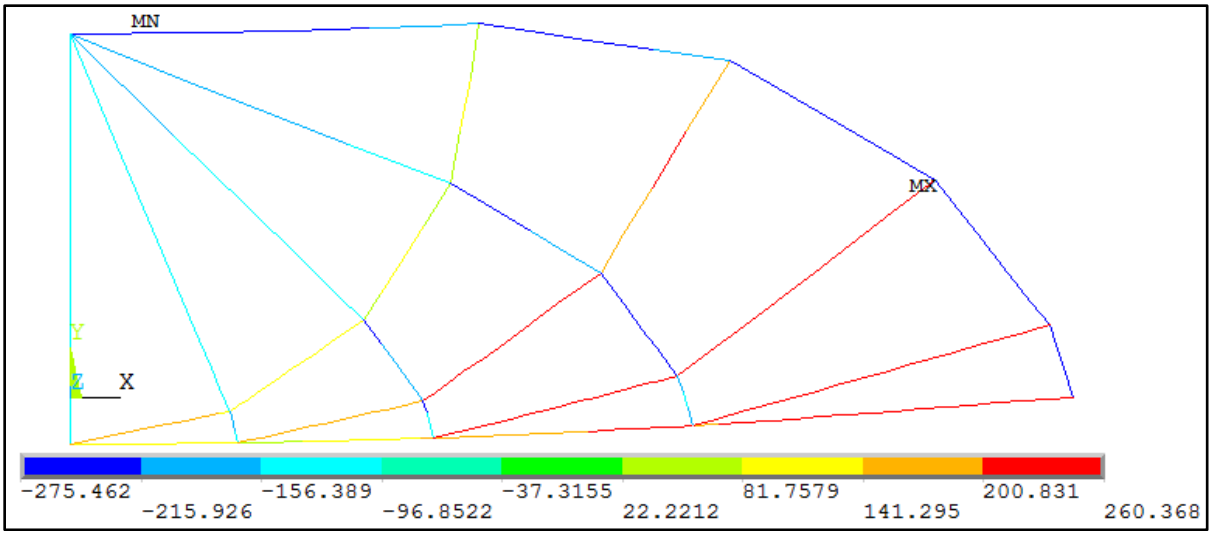

Figure 9.5 Minimum Stress Distribution for Optimized Design

9.5 Comparison of Mass results

The truss volume reported in the published reference (28) is 275 cm^3. For aluminum, this results in a mass of 743g for the entire model and 371 g for half of the model. This value

is lower than the mass of the optimum truss which was found to be 522 g. However, the published reference truss does not have a uniform width. In Figure 9.6 the outer top strut has a full width of 25 mm while the internal struts are somewhat smaller. Three specific regions are circled in red that show this difference in width. The strut thicknesses are also different throughout the truss. An exact mass comparison could not be determined because the thickness and width of each strut were not provided.

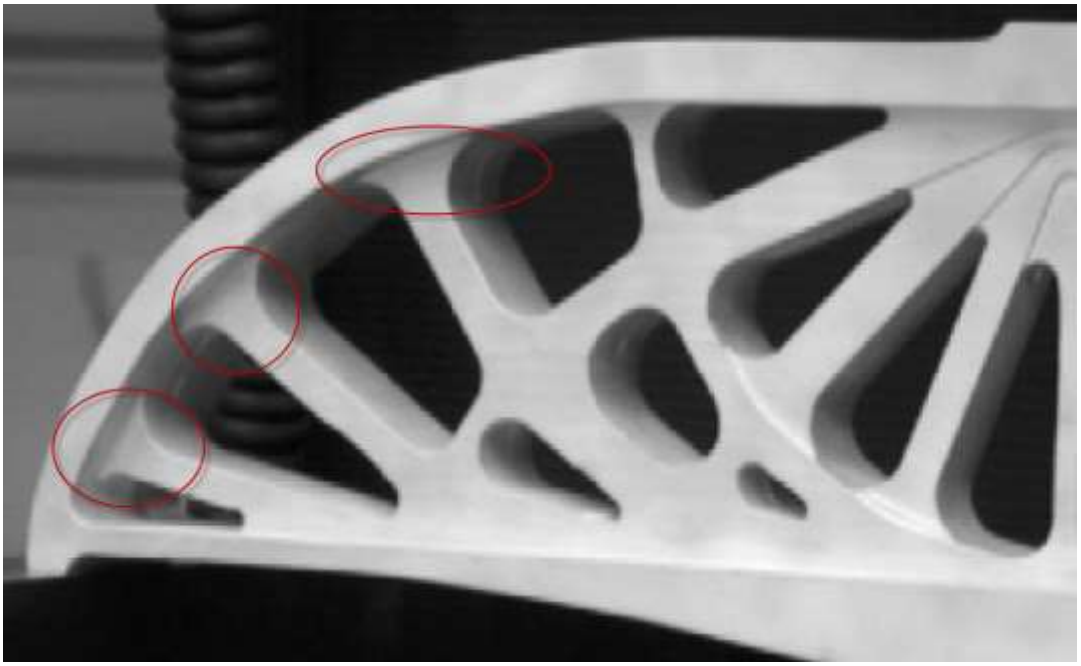

Figure 9.6 Different Depths for Different Struts in Published Results

The robustness of the optimization algorithm was tested by determining if the optimum mass solution would change if different starting strut thicknesses were used. Three starting designs were used where all struts had a constant thickness of 5 mm, 10 mm, and 15 mm in the optimization algorithm. Table 9.1 shows a comparison of the final fitness and the standard deviation for each set of runs.

Table 9.1 Comparison of Optimum Design Mass for Different Starting Thicknesses

Fitness	Run1(g)	Run2 (g)	Run3 (g)	Standard Deviation
5 mm	571	557	559	8.02
10 mm	563	571	558	6.56
15 mm	561	565	565	2.55

In all cases, the maximum stress does not exceed the yield strength. Hence, the fitness is equal to the mass. As expected, there are small differences in the final mass. For each of the three starting thicknesses, the average thickness is calculated from the three runs and compared in Figure 9.7. The final thickness values for a given strut are approximately equal irrespective of the starting point. There are some anomalies such as struts 19 and 24, which show a higher thickness for the first run. This behavior is expected since a heuristic optimization approach was used. The final thicknesses for all runs are shown in the appendix.

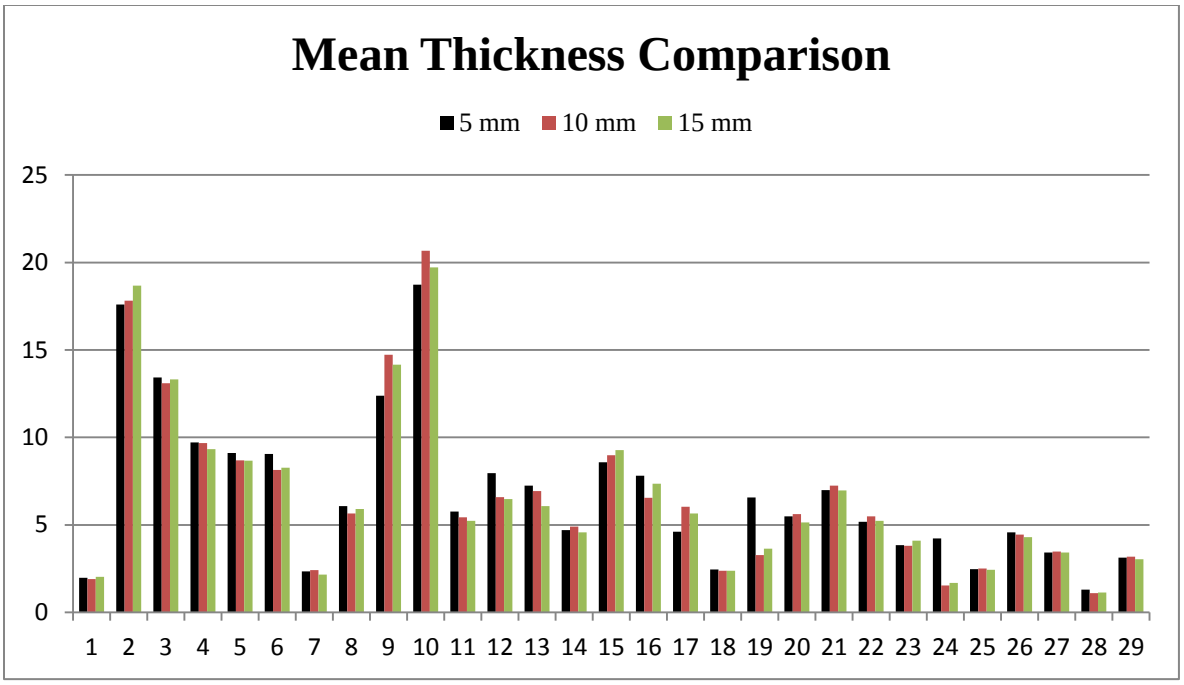

Figure 9.7 Thicknesses of Struts Compared with Different Starting Thicknesses

9.6 Deformation Results

The maximum deflection of the optimized beam was found to be 2.05 mm. This value is smaller than the experimental reference beam (28). Since the beam model will have overlapping material, a finite element analysis was conducted using the optimized thicknesses. Tetrahedral elements were used. The force, constraints and mesh are shown in Figure 9.8. The direct sparse solver in SolidWorks Simulation was used in this analysis.

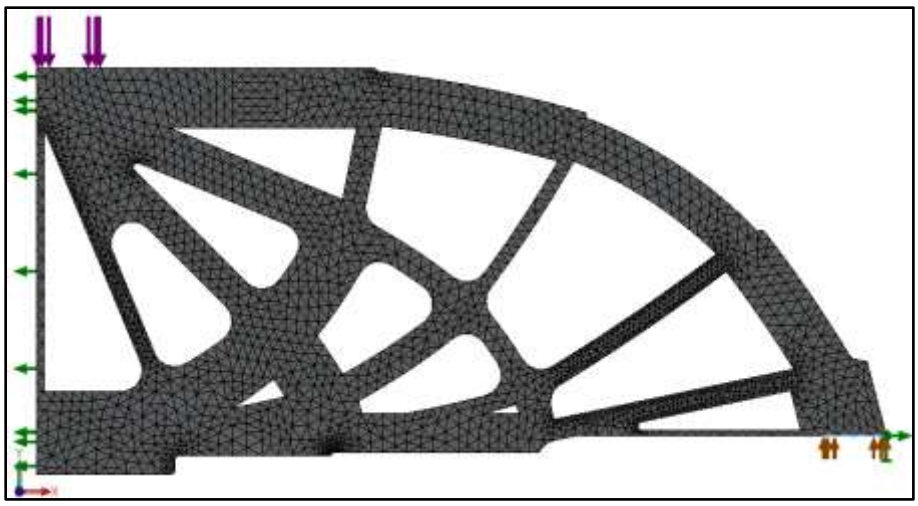

Figure 9.8 CAD Model of Optimized Beam

The deformation plot for this model is shown in Figure 9.9. The maximum deflection is at the point of the load and it is equal to 2.35 mm.

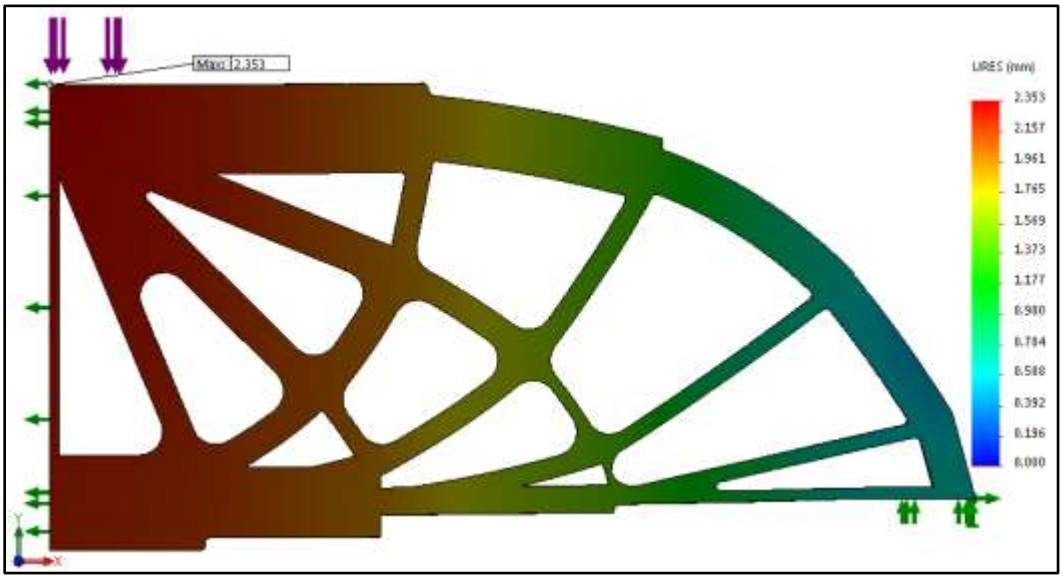

Figure 9.9 Deformation Results for Tetrahedral Mesh

The maximum deformation in the CAD model without overlapping material is a more accurate representation and it is closer to the experimental results with an error of approximately 7%.

9.7 Additive Manufacturing Constraints

The previous results were generated without considering AM constraints. The same optimization study was conducted with a starting thickness of 5 mm for all the struts with AM constraints on the minimum thickness and penalty for the separation of adjacent struts below suggested clearance limits. The results for the optimum beam are summarized in Table 9.2.

Table 9.2 Optimized Model Characteristics with AM Constraints

Starting Thickness	Mass of half model	Mass of half CAD model
5 mm	572 g	526 g
Fitness	Max Stress	Max Deflection
572 g	275.75 MPa	1.98

The mass of this beam from the optimization algorithm is similar to the mass calculated previously without AM constraints. The clearance limit as described in Chapter 8 for the different lines was also included and a penalty was added to the fitness for any violations. Figure 9.10 shows that there were several constraint violations that occurred during the early iterations. However, no violations in the clearance limit were noticed after about iteration 100 and until the final iteration.

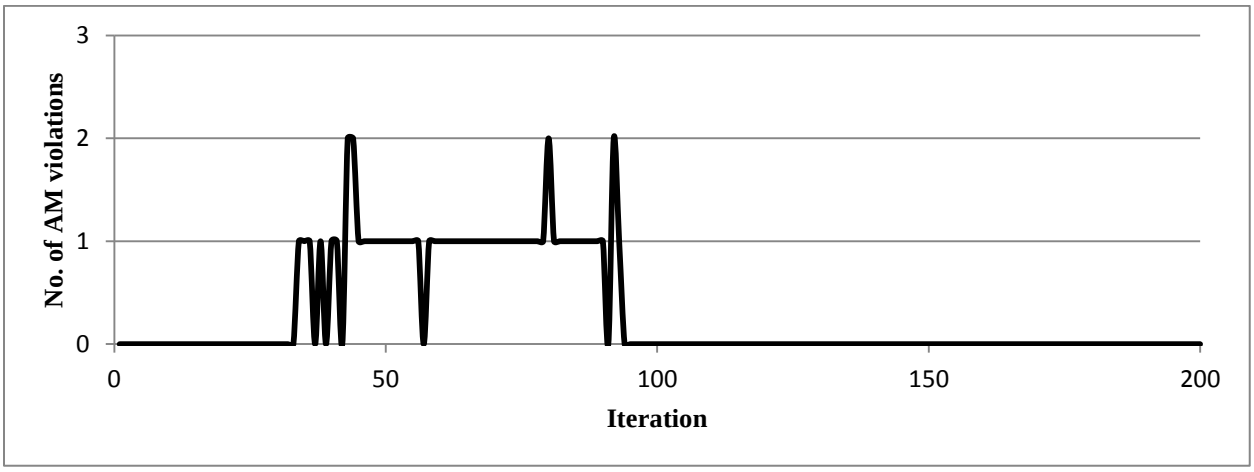

Figure 9.10 Additive manufacturing Violations vs Iteration

The optimized design is relatively similar to the results displayed in the beginning of this section in which AM constraints were not used. Also, the earlier thicknesses are checked and no constraint was violated. There are points in the middle of the graph in Figure 9.10 where AM constraints were violated. This increases the overall fitness value of those designs.

Beam designs with large thicknesses will have no stress violations but they will result in a larger mass. Incorporating AM constraints will increase the fitness of these designs because the larger strut thicknesses have a higher probability of violating AM constraints. Therefore, even though the final design is not affected by the new constraints, the algorithm is able to find a better design faster because of additional penalties for poorer designs.

The minimum thickness limit for all design variables imposed by the AM constraints in this analysis do not affect the solution because the thicknesses in the optimum design are above the minimum limit. If the direction of build was not along the constant cross section, the angle constraint would still affect only the initial topology since the algorithm only finds the thickness of each strut and doesn't change the angle.

9.8 Summary

The optimum results presented in this chapter are very similar to the results reported in Reference (28). The maximum deformation is smaller because the beam model stiffness is larger. To account for overlapping material, a 3D CAD model was created using the thicknesses of the optimized truss, and the deformation was determined using tetrahedral elements. Here, a small 5% error was found for the maximum deformation when compared to the published Reference (28). Due to the nature of the two-dimensional analysis, there were high stress values above yield near the constrained faces. In such cases, the deformation is a conservative estimate of the actual deformation. For the beam model, the maximum tensile and maximum compressive stresses were nearly equal to the yield strength limit of 276 MPa. Hence, the design is close to the global optimum.

As described previously, none of the optimum beam designs had AM constraint violations. However, the AM constraints helped the algorithm converge to an optimum solution sooner, because bad designs were penalized with larger strut thicknesses.

Due to the nature of the simulated annealing algorithm, bad designs are initially accepted. This can lead to the loss of several good designs. However, by accepting bad

designs the algorithm gains the ability of not getting stuck at a local minima and not being affected by the starting thickness of all struts.

An exact comparison of the optimum beam solution in this thesis with the reference beam could not be achieved because complete cross-sectional areas of the struts were not reported. To demonstrate the robustness of the algorithm three constant starting thickness values of 5 mm, 10 mm, and 15 mm were chosen and three runs from each point were conducted. The mass and thickness characteristics of the final optimum beam design were compared and only minor differences are noticed as expected since a heuristic approach was used.

10. POINT LOAD CANTILEVER BEAM

10.1 Introduction to a Point Load Cantilever Beam

In the earlier chapters, a Michell truss as defined by slip lines was introduced as an optimized lattice structure. An optimization algorithm was developed and additive manufacturing constraints were applied to find the minimum weight beam. In this chapter, this optimization technique is applied to a cantilever beam with an end point load.

10.2 Initial Michell Truss Shape

As shown in Figure 10.1, a cantilever beam is fixed on the left end and a point load is applied along the neutral axis at the right end. This cantilever beam is 60mm wide, 10mm deep and 30mm tall. The principal stresses are determined using the FEA SolidWorks Simulation software. Tetrahedral elements and a direct sparse solver were used to solve for the stresses. Note that the principal stress directions at a given point do not change direction whereas the magnitude of the principal stresses can change with the value of the applied force.

Figure 10.1 Cantilever Beam Loading Conditions

The maximum and minimum principal stress trajectories are shown in Figure 10.2.

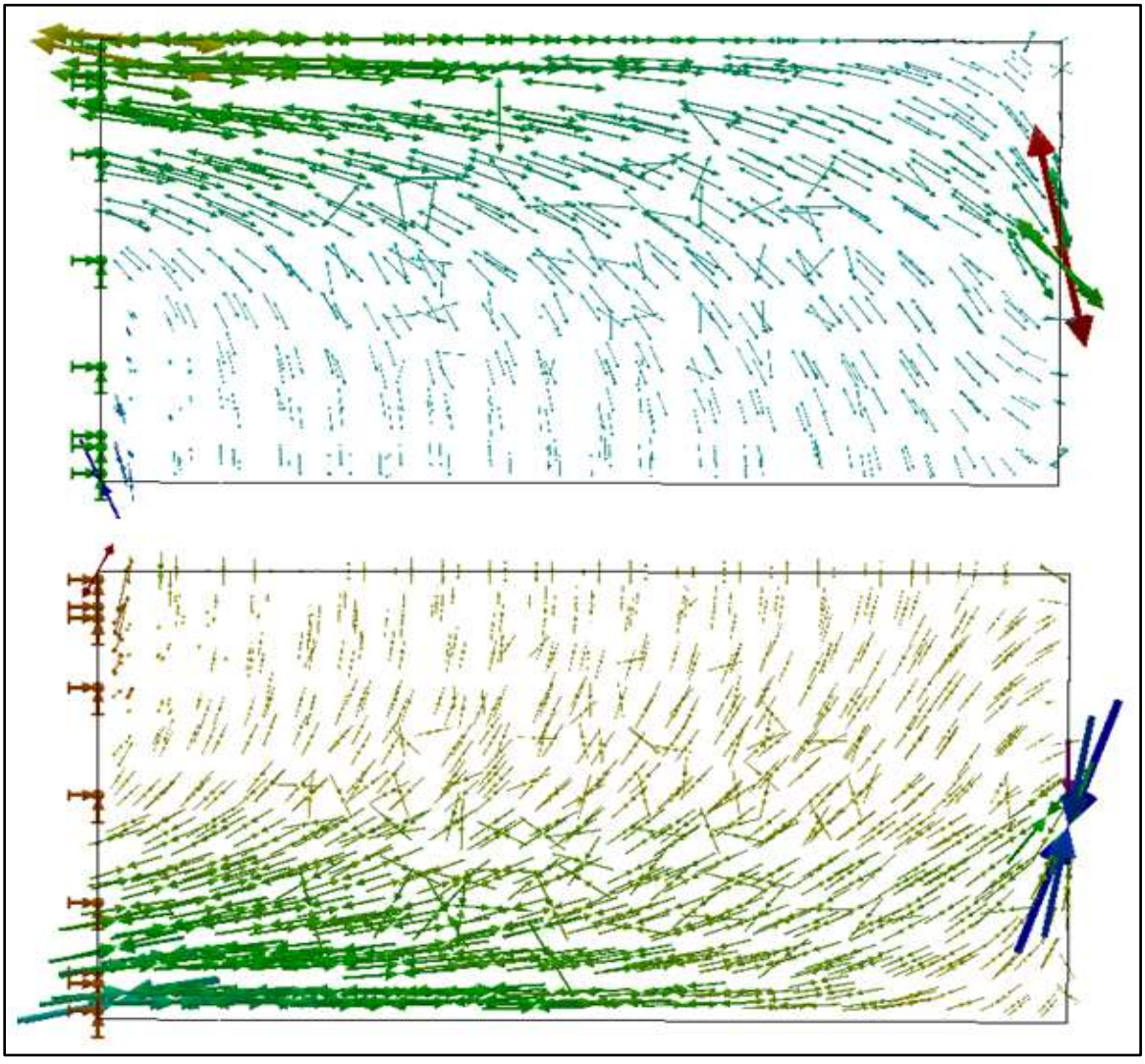

Figure 10.2 Maximum and Minimum Principal Stress Trajectories

The above stress trajectories provide a general sense of the slip lines and directions of the material in the interior of the cantilever beam. At this point, the direction of the slip lines has been determined. The number of slip lines to be used is coupled with the thickness of each line and is at the discretion of the designer and the resolution of the AM process. Figure 10.3 shows the final topology of the part as chosen by the author. A common thickness is applied which has not been optimized in this figure. The thickness of each strut is currently held constant and will be optimized next. The alpha and beta lines intersect each other at a 90^{o} degree angle. All lines intersect the neutral axis at 45^{o}.

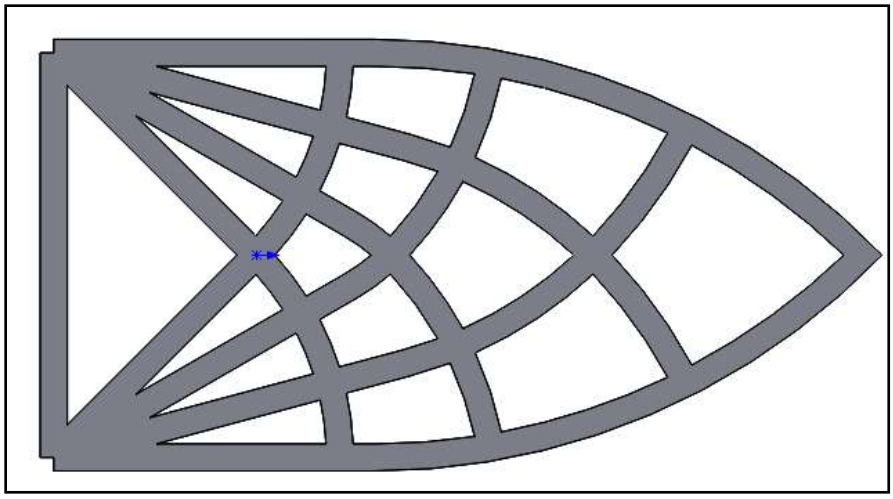

Figure 10.3 Cantilever Beam Model Topology

Figure 10.4 shows a general shape of a cantilever beam with a point load published by Lewinski (46). The direction of the alpha and beta lines chosen for the topology in Figure 10.3 is in agreement with these published results.

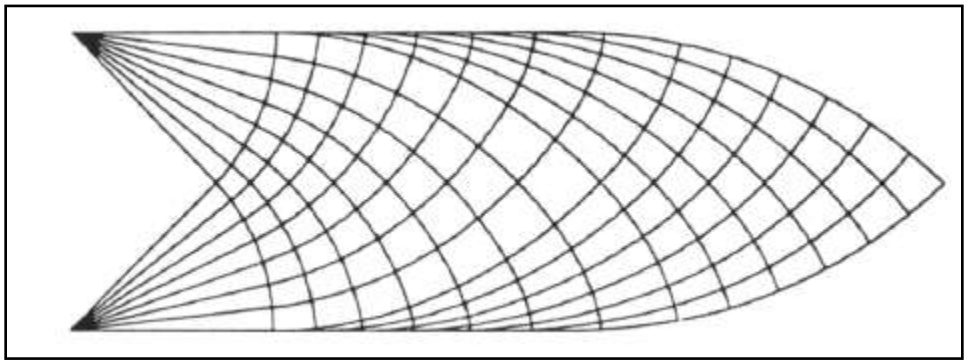

Figure 10.4 Michell Truss for Cantilever Beam with Point Load (46)

10.3 Finite Element Model

A finite element model of the beam was developed using BEAM3 elements. The length and width of all struts are held constant. The thicknesses of the struts constitute the design variables. The ANSYS model is shown in Figure 10.5. The left line is fixed and a force of 4000N is applied at the right most point. The material is aluminum 6061 T6. The model is constrained by fixing the left most line. Due to the beam model setup, no stress will be seen in this line. Hence, it is held at a constant thickness of 3 mm.

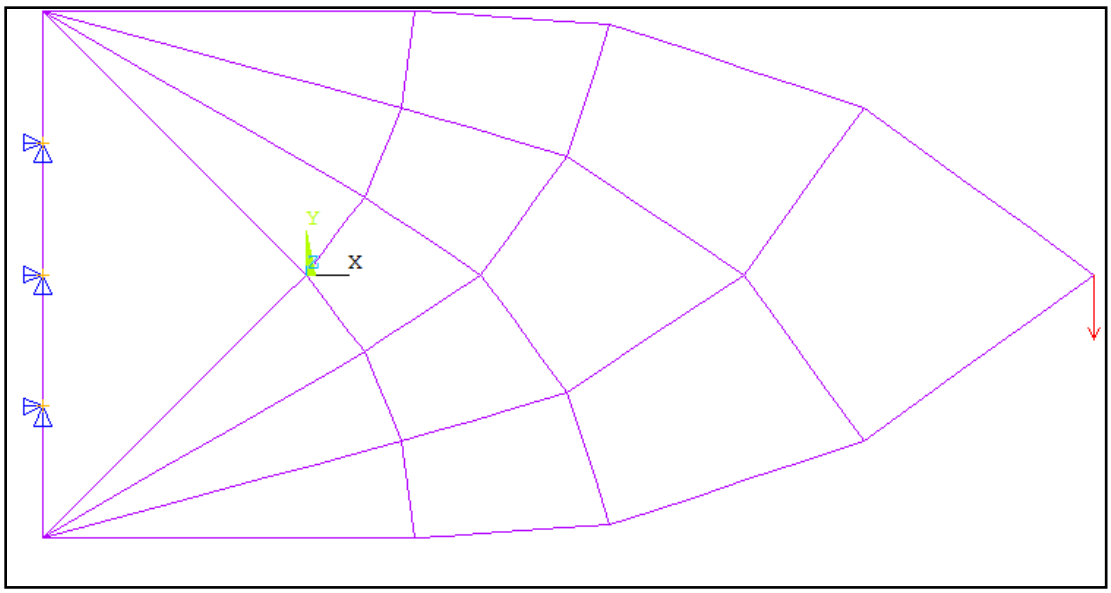

Figure 10.5 FEA Setup for Point Load Cantilever Beam

10.4 Optimization algorithm

To optimize the thickness of each strut in the beam, a similar optimization algorithm was used as for the symmetrical simply-supported beam. There are 32 struts and the thicknesses of each of these lines represent the design variables that will be determined by the algorithm. The problem formulation is as follows:

Minimize: $Mass = \rho * depth * \sum(length\ (i) * thickness\ (i))$

Subject to: $Stress\ value\ (i) - \sigma_y <= 0$

$Thickness\ (i) > 0$

$Additive\ Manufacturing\ constraints\ stated\ below$

The general flow of the algorithm is described in Chapter 7. For each set of design variables, ANSYS is used to calculate the stress and penalty. The mass is calculated by finding the volume and multiplying it with the mass density. The depth and length of all lines are held constant. To account for constraints, two penalties are calculated for the stress and additive manufacturing constraints, respectively. These penalties are added to the mass to determine the fitness. The objective of the study is to minimize the fitness or equivalently, minimize the mass.

10.5 Parameters and Constraints

Aluminum 6061 T6 has a yield strength of 276 MPa which was used as the material strength. To account for additive manufacturing constraints, upper and lower bounds were selected for the thicknesses. A range of 1 mm and 5 mm was selected. The 1 mm thickness limit is based on AM constraints as described in Chapter 8.

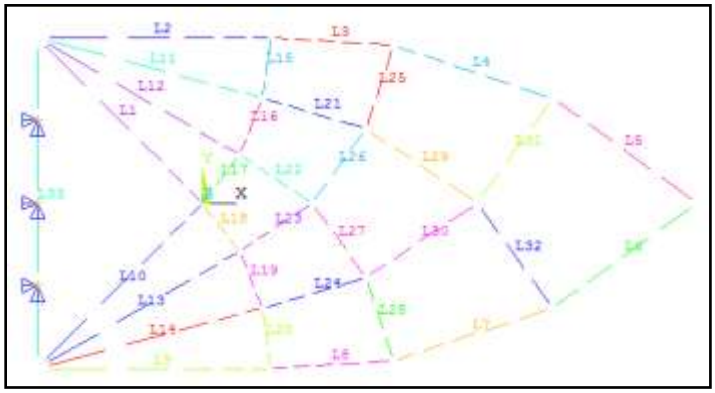

Figure 10.6 Line Numbers of Additive Manufacturing Constraints

There should also be a minimum clearance of 0.5 mm between nearby trusses. The midpoints of adjacent struts were found and their separation distance was calculated. Figure 10.6 shows the line numbers and Table 10.1 shows the minimum distance required between them.

Table 10.1 Distance Calculations for AM Constraints

Alpha Lines	Distance (mm)	Beta Lines	Distance (mm)
L18-L22	6.71	L8-L24	6.9
L21-L22	6.76	L23-L24	6.8
L3-L21	6.86	L17-L23	6.7
L19-L27	8.9	L30-L7	9.7
L29-L27	10.3	L30-L26	10.3
L4-L29	9.1	L16-L26	8.9
L20-L28	10.54	L6-L31	14
L28-L32	13.75	L25-L31	13.8
L5-L32	14	L15-L25	10.5

10.6 Results

A thickness of 2.5 mm was set as the initial thickness for all struts. Figure 10.7 shows the change in fitness as a function of the iterations. The initial designs have a higher probability of accepting bad design which results in spikes in the fitness. As the iterations increase, fewer bad designs are accepted. After 300 iterations, there are only small changes in the fitness which indicates that convergence has been reached. The mass of the optimized design was found to be 34g and there were no stresses that exceeded the yield strength.

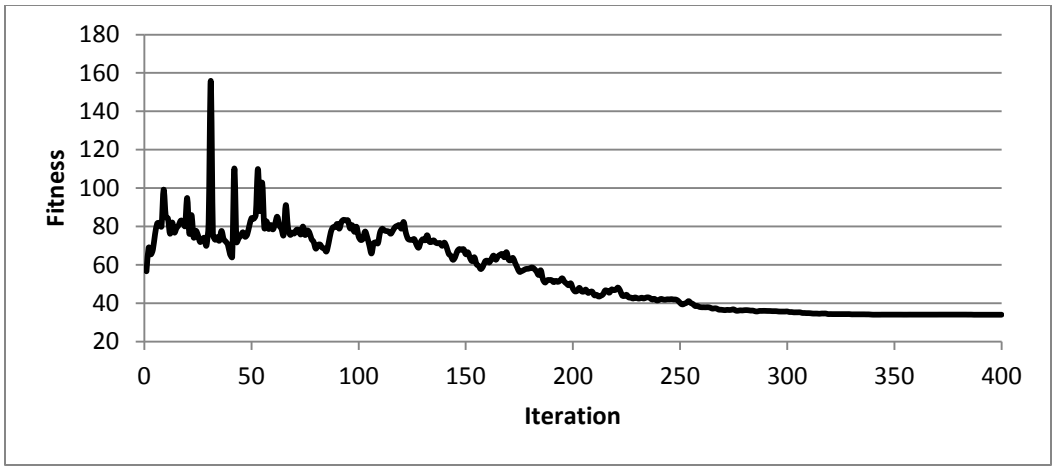

Figure 10.7 Fitness vs Iteration

10.7 Stress Results

The maximum tensile stress is shown in Figure 10.8. As expected, the alpha lines exhibit higher tensile stress.

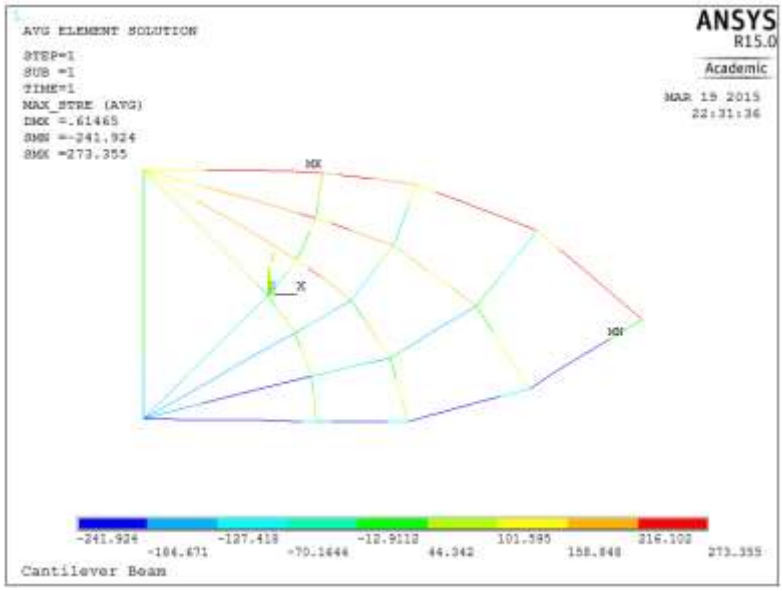

Figure 10.8 Tensile Stress for the Optimum Beam

The minimum stress or maximum compressive stresses are higher for the beta lines as shown in Figure 10.9.

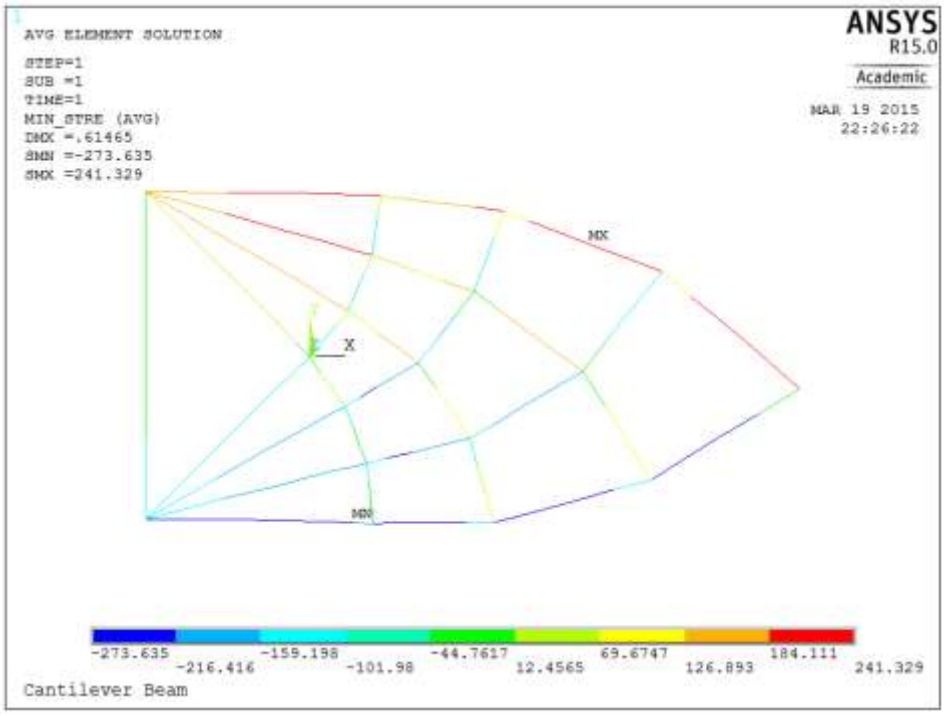

Figure 10.9 Compressive Stress for the Optimum Beam

The absolute values of both stresses are less than the yield strength of 276 MPa. Hence, the optimized model does not have any stress violations. The maximum stress as a function of the iterations is shown in Figure 10.10. The stress initially fluctuates between designs that exhibit penalties and bad designs with larger thicknesses. As the penalty is increased, stress violations occur less frequently and the solution converges to a design with small strut thicknesses in which the stresses are slightly less than the yield strength.

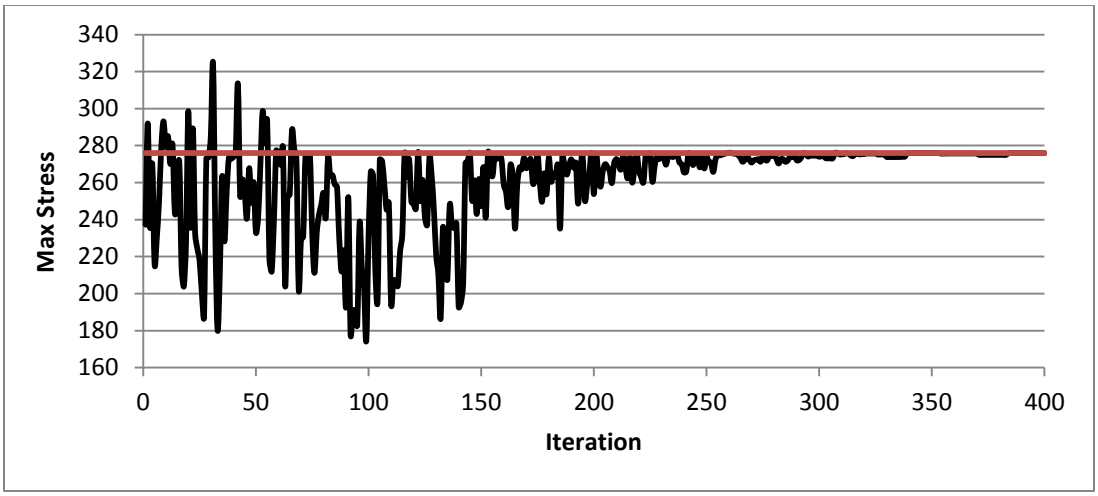

Figure 10.10 Maximum Stress vs Iteration

10.8 Optimized Beam Deformation

Figure 10.11 shows the optimum beam CAD model. All thicknesses are between 1 mm and 2 mm. Most struts have a thickness just above the 1 mm minimum limit set due to additive manufacturing constraints. Note that if the AM constraints had not been included, the strut thicknesses would have been less than 1mm.

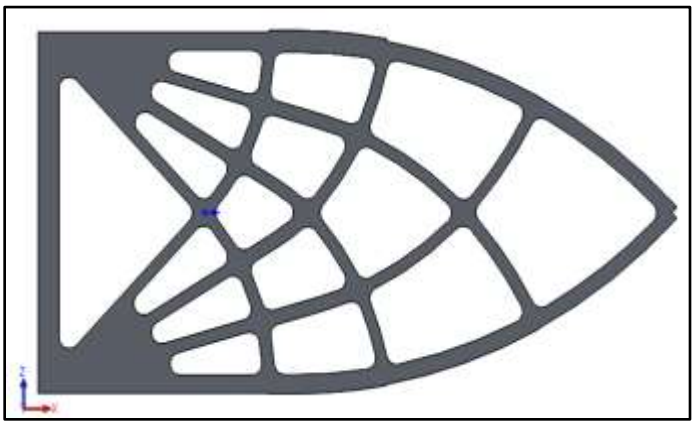
Figure 10.11 Optimum Beam CAD Model

In general, the model exhibits uniform thickness transitions along both the alpha and beta lines. Only one strut that is located on the top is slightly thicker than the others. None of the additive manufacturing constraints were violated.

The maximum deformation of the beam model is 0.61 mm as shown in Figure 10.12. For comparison, a plane stress model using triangular elements was developed and it was used to calculate the maximum deformation which was found to be 0.66 mm.

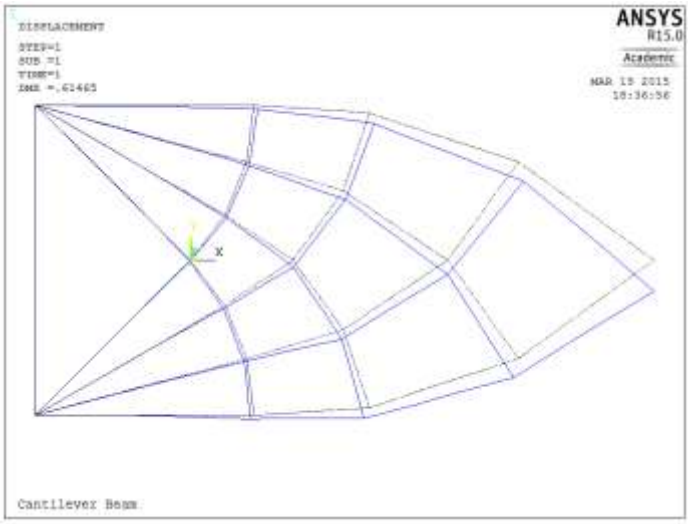

Figure 10.12 Deformation of the Optimum Beam

10.9 Comparison of Results with Existing Design

The optimum shape of the cantilever beam developed in this thesis is compared with an existing solution of a cantilever beam designed using a different optimization technique. Huang (47) found an optimum shape for a cantilever beam by taking mean compliance and

volume fraction into account and using some of the techniques described in Section 4. The setup for both cantilever beams is the same although different dimensions and forces are used. The change in shape as a function of the algorithm is shown in Figure 10.13. The time taken to solve for the optimum was not reported in Reference (47).

Comparing the final shape on the right top of the above figure with the shape developed in this thesis, several notable comparisons can be observed. The outer struts align in a similar shape in both designs. They are horizontal at the left and change to a 45^{o} angle at the point of the load at the intersection with the neutral axis. Also, the outer struts in both cases have a higher thickness value as compared to the inner struts. In Huang's paper (47) the thickness of the different regions is found by using an algorithm that either adds or removes material.

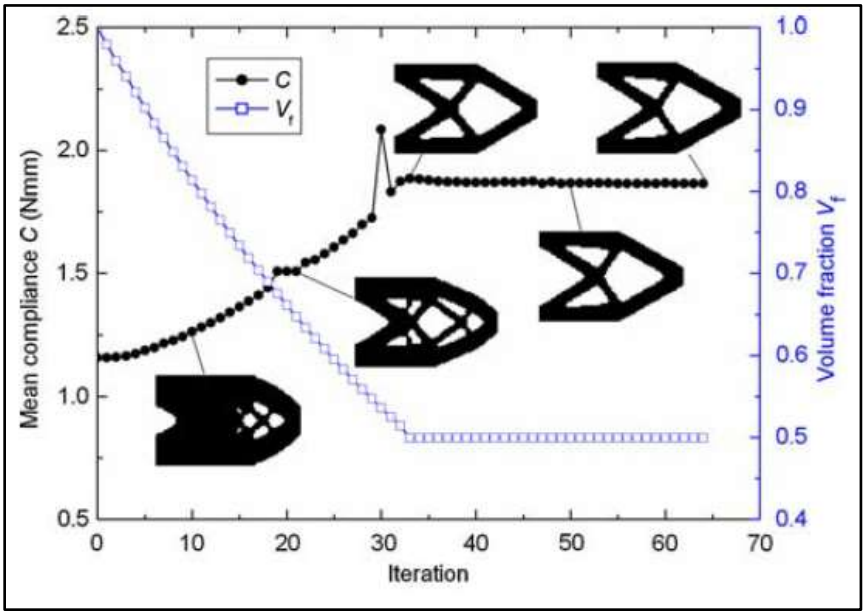

Figure 10.13 Cantilever Beam Optimum Shape (47)

Four slip lines were chosen in this thesis for the initial topology and the thickness for each line was found. Figure 10.13 has fewer internal lattice struts with one internal line in tension and one line in compression. It is seen that these lines follow a path similar to a slip line field as defined by Michell's truss theory. Another similarity is that the internal lattice tension and compression lines are also perpendicular to each other. In addition, they intersect the neutral axis at a 45^{o} angle.

From this comparison, it can be inferred that a slip line field is a convenient method for determining the initial topology of a beam with minimum mass. The optimization algorithm can be used to find the thickness of the struts based on the initial topology. For the chosen initial topology and the applied manufacturing constraints, the beam shown in Figure 10.11 is designed for minimum mass. For similar manufacturing considerations, it is possible to further reduce the mass if a different initial topology was used.

10.10 Discussion

A minimum mass solution for a cantilever beam was achieved with no stress violations and the fitness converged after 400 iterations. Several strut thicknesses reached the lower limit of 1 mm which was set by the additive manufacturing constraints.

The compliance of the cantilever beam needs to be taken into consideration when designing such a structure. If the applied force is increased by a large amount, the finite element assumptions of small deformations might be violated and the analysis will not be accurate. Optimization algorithms with compliance constraints have been published in the past. For large forces, the compliance constraint could be the limiting factor of such a design.

Another consideration between the beam model and the plane stress model is the difference in stresses. The plane stress model had higher stress in localized regions near the supports. To account for these, it is advisable to use a factor of safety in the optimization algorithm which would allow for higher localized stresses without exceeding the yield strength.

In this chapter, a cantilever beam of given outer dimensions with a point force was analyzed. The initial topology including an internal lattice was defined using principal stress trajectories. The thicknesses of the struts were calculated using a simulated annealing optimization algorithm. Additive manufacturing constraints including clearance limits and minimum allowable thicknesses were incorporated into the algorithm.

11. CONCLUSION

The objective of this thesis was to create a topology optimized design using a Michell truss layout while also accounting for additive manufacturing constraints. Simulated annealing was applied to the design of a minimum weight lattice that could be made with the additive manufacturing processes. A Michell truss was used as the basis for the lattice. It has been shown that the layout of a Michell truss coincides with the principal stress trajectories. However, these intricate lattices are difficult to manufacture with traditional methods. A more promising approach is to use additive manufacturing for complex parts. A new and general method for determining slip lines in a Michell truss was introduced using a finite element plane stress model. The trajectories of the maximum and minimum principal stress directions are coincident with the slip lines and hence, these trajectories provide the layout of a Michell truss. An optimization algorithm was then used to find the thicknesses of all the struts within the Michell truss.

The minimum weight design for a simply-supported Michell truss was determined and then compared with published results. Excellent agreement was found between the optimized strut thicknesses and Reference (28). Finally, a small difference of approximately 5% was found for the overall deformation.

Constraints for additive manufacturing were also incorporated in the optimization algorithm. The initial design is bounded by the maximum and minimum allowable dimensions of the 3D printer. The limits for allowable values of the design variables are governed by the tolerances of the additive manufacturing process. Also, a penalty was

introduced when clearance limits between slip lines were violated which helped guide the design towards a minimum weight solution while satisfying additive manufacturing constraints.

The generality of the optimization algorithm was demonstrated by using it to determine the minimum weight design of a cantilever beam with a point load. The internal lattice was first defined by finding the maximum and minimum principal stress trajectories. Once the topology was defined, the strut thicknesses were found using the optimization algorithm.

In summary, a powerful optimization technique was developed in this thesis that can be used to design a minimum weight Michell truss. Complex lattice structures can be designed and then manufactured with AM processes that incorporate known manufacturing tolerances. The technique can also be used to maximize the stiffness of a structure for a given mass.

12. RECOMMENDATION FOR FUTURE WORK

Simulated annealing was used for all of the optimization analyses in this thesis. This is a versatile heuristic approach. Other heuristic techniques exist that were not explored. These include techniques such as Genetic Algorithms and Particle Swarm Optimization. These techniques could result in more rapid convergence to an optimized solution.

The optimization technique developed in this thesis focused on determining the strut thicknesses for a known layout. The layout and the solution for the thicknesses are actually coupled and an algorithm could be developed for designing a lattice with both an optimum layout and strut thicknesses. It is anticipated that as more slip lines are used, the thickness of each would be decreased. However, this could result in the violation of AM constraints for the minimum thicknesses and the clearance between adjacent struts.

Improvements in the finite element model could also be introduced. In this thesis, beam elements in ANSYS were used, which do not account for localized stresses that occur at the point of load, boundary conditions and at the intersection of struts. New element types could be introduced that more accurately represent these stresses.

Finally, new AM constraints could be considered as the technology of additive manufacturing continues to advance. For example, this might include new materials that do not exhibit linear material properties. Other constraints might include the direction of the build and the use of supporting material during the build that is not part of the final design.

13. REFERENCES

1. Doubrovski, Z., Jouke, C. C., & Geraedts, J. M. P. (2011). Optimal design for additive manufacturing: Opportunities and challenges. ASME IDETC/CIE 2011, Washington, DC.

2. Rozvany, G. I. N. Some shortcomings in michell's truss theory. (Structural Optimization), 203-204.

3. Michell, A. G. M. (1904). The limits of economy of material in frame structures. VIII - Sixth Series, 589-597.

4. Campbell, I., & Wohlers, T. (2014). Direct part production: Design for AM. Wohlers report 2014 (pp. 176-177). Fort Collins, Colorado: Wohlers Associates.

5. A third industrial revolution. (2012). Retrieved from http://www.economist.com/node/21552901

6. Solid print: Making things with a 3D printer changes the rules of manufacturing. (2012). Retrieved from http://www.economist.com/node/21552892

7. Bourell, D., Beaman, J., Leu, M. C., & Rosen, D. (2009). A brief history of additive manufacturing and the 2009 roadmap for additive manufacturing: Looking back and looking ahead. Proceedings of RapidTech, , 24-25.

8. Jariwala, A. S., Ding, F., Zhao, X., & Rosen, D. W. (2009). A process planning method for thin film mask projection micro-stereolithography. Paper presented at the ASME 2009 International Design Engineering Technical Conferences and Computers and Information in Engineering Conference, 685-694.

9. Bourell, D., Hopkinson, N., & Beaman, J. (2014). Part 7: Research and development. Wohlers report 2014 (pp. 191). Fort Collins, Colorado: Wohlers Associates.

10. Suresh, K. (2014). Efficient microstructural design for additive manufacturing. ASME IDETC/CIE 2014, Buffalo, NY. (ASME 2014 IDETC)

11. 3D ops. Retrieved from http://3dops.co/#

12. Hope you trust 3D printers - Boeing uses them to 'print' parts for its planes. Retrieved from http://www.businessinsider.com/boeing-uses-3d-printers-for-airplane-parts-2013-6

13. 3D printed LEAP engines successfully take to the sky. (2014). Retrieved from http://3dprintingindustry.com/2014/10/13/ge-3d-printed-leap-engines/

14. GE additive manufacturing. Retrieved from http://www.ge.com/stories/advanced-manufacturing

15. Electron beam melting - in the forefront of additive manufacturing. Retrieved from http://www.arcam.com/technology/electron-beam-melting/

16. FDM technology. (2015). Retrieved from http://www.stratasys.com/3d-

17. Formlabs materials. (2015). Retrieved from http://formlabs.com/en/products/materials/standard/

18. Maxwell, C. (1890). Scientific papers II, comb. univ. press, 175-176,177.

19. Rozvany, G. I. N., & Lewinski, T. In Pfeiffer F., Rammerstorfer F. G. and Guazzeli E. (Eds.), (Topology optimization in structural and continuum mechanics) Vol. 549 ed., Springer.

20. Cox, H. (1958). The theory of design. Cited by W.S. Hemp.

21. Hemp, W. (Aug 1958). Theory of the structural design: Report No. 115(College of Aeronautics)

22. Rice, J. R., & Sorensen, E. P. (1968). Continuing crack-tip deformation and fracture for plane-strain crack growth in elastic-plastic solids, 26 (Journal of the Mechanics and Physics Solids), 163-186.

23. Ewing, D. J. F. (1967). A series-method for constructing plastic slipline fields, 15 (Journal of the Mechanics and Physics of Solids), 105-114.

24. Dewhurst, P. (2000). Analytical solutions and numerical procedures for minimum-weight michell structures. (Journal of the Mechanics and Physics of Solids), 445-445-467.

25. Hemp, W. (1973). Optimum structures Oxford: Clarendon.

26. Deaton, J. D., & Grandhi, R. V. (2014). A survey of structural and multidisciplinary continuum topology optimization: Post 2000. (Structural and Multidisciplinary Optimization), 49(1), 1-38.

27. Zhou, M., & Rozvany, G. (1991). The COC algorithm, part II: Topological, geometrical and generalized shape optimization. (Computer Methods in Applied Mechanics and Engineering), 89(1), 309-336.

28. Srithongchai, S., Demircubuk, M., & Dewhurst, P. (2002). A theoretical and experimental investigation of a family of minimum-weight simply-supported beams. (International Journal of Mechanical Sciences), 37-55.

29. Strömberg, N. (2010). An efficient tradeoff approach for topology optimization with manufacturing constraints. Paper presented at the ASME 2010 International Design Engineering Technical Conferences and Computers and Information in Engineering Conference, 1171-1179.

30. Eschenauer, H. A., & Olhoff, N. (2001). Topology optimization of continuum structures: A review*. (Applied Mechanics Reviews), 54(4), 331-390.

31. Eschenauer, H. A., Kobelev, V. V., & Schumacher, A. (1994). Bubble method for topology and shape optimization of structures (Structural Optimization), 42-51.

32. Haftka, R. T., & Grandhi, R. V. (1986). Structural shape optimization—a survey. (Computer Methods in Applied Mechanics and Engineering), 57(1), 91-106.

33. Bendsøe, M. P. (1989). Optimal shape design as a material distribution problem. (Structural Optimization), 1(4), 193-202.

34. Suzuki, K., & Kikuchi, N. (1991). A homogenization method for shape and topology optimization. (Computer Methods in Applied Mechanics and Engineering), 93(3), 291-318.

35. Jog, C. S., & Haber, R. B. (1996). Stability of finite element models for distributed-parameter optimization and topology design. (Computer Methods in Applied Mechanics and Engineering), 130(3), 203-226.

36. Arora, J. S. (2004). Introduction to optimum design (2nd ed.). San Diego, CA: Elsevier.

37. Eberhart, R. C., & Kennedy, J. (1995). A new optimizer using particle swarm theory. Paper presented at the Proceedings of the Sixth International Symposium on Micro Machine and Human Science, 1 39-43.

38. Melchers, R. (2005). On extending the range of michell-like optimal topology structures. (Structural and Multidisciplinary Optimization), 29(2), 85-92.

39. Dewhurst, P., & Collins, I. (1973). A matrix technique for constructing slip-line field solutions to a class of plane strain plasticity problems. (International Journal for Numerical Methods in Engineering), 7(3), 357-378.

40. Barnett, R. L. (1966). Survey of optimum structural design. (Experimental Mechanics), 6(12), 19A-26A.

41. Gere, J. M., & Timoshenko, S. P. Application of plane stress. (Mechanics of materials) 4th ed., pp. 563-566. Boston, MA: PWS Publishing Company.

42. Hasançebi, O., & Erbatur, F. (2002). Layout optimisation of trusses using simulated annealing. (Advances in Engineering Software), 33(7), 681-696.

43. Brackett, D., Ashcroft, I., & Hague, R. (2011). Topology optimization for additive manufacturing. Paper presented at the 22nd Annual International Solid Freeform Fabrication Symposium, 348-362.

44. Design specification for alumide. (2015). Retrieved from http://i.materialise.com/materials/alumide/design-guide

45. DMLS design guidelines. (2015). Retrieved from https://www.solidconcepts.com/resources/design-guidelines/dmls-design-guidelines/

46. Lewiński, T., Zhou, M., & Rozvany, G. (1994). Extended exact solutions for least-weight truss layouts—part I: Cantilever with a horizontal axis of symmetry. (International Journal of Mechanical Sciences), 36(5), 375-398.

47. Huang, X., & Xie, Y. (2009). Bi-directional evolutionary topology optimization of continuum structures with one or multiple materials. (Computational Mechanics), 43(3), 393-401.

APPENDICES

A. Thickness Comparison for Different Starting Points

The optimization algorithm is expected to converge from different starting points. The three graphs below show the final optimum thickness value of each of the struts when the starting thickness is 5mm, 10mm and 15mm.

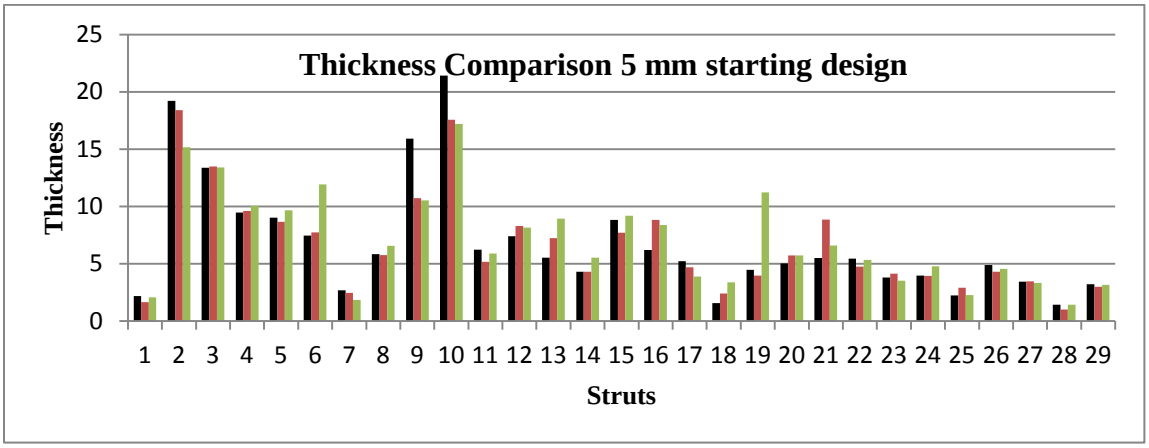

Figure A.1 Thickness Comparison of optimum design struts with 5 mm starting thickness

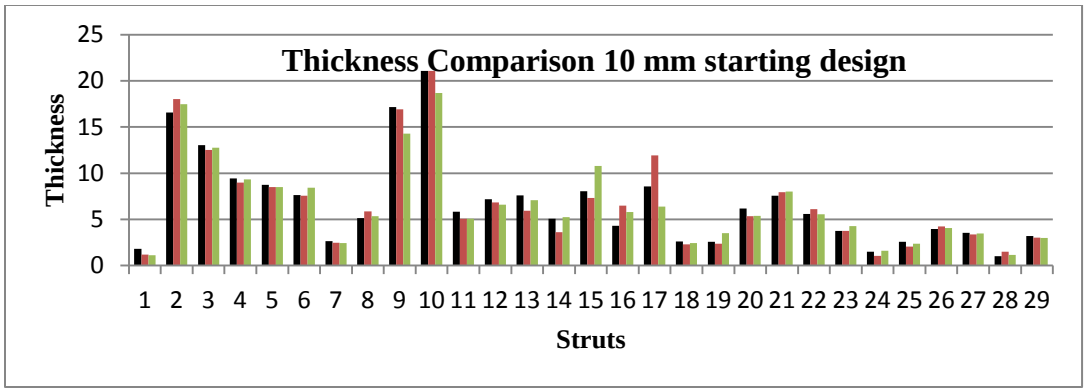

Figure A.2 Thickness Comparison of optimum design struts with 10 mm starting thickness

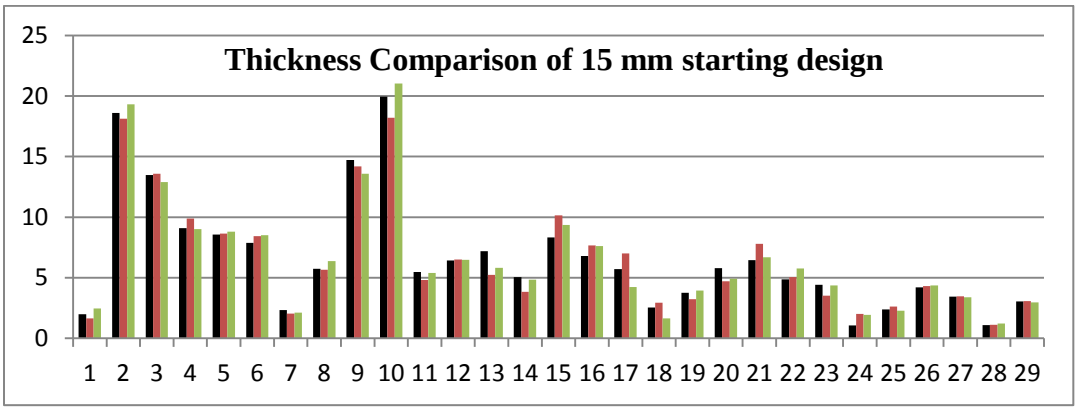

Figure A.3 Thickness Comparison of optimum design struts with 15 mm starting thickness

B. Optimized Design ANSYS Input Text File

Simply-Supported Beam

```
FINISH
/PREP7
/TITLE, Michell Truss
ANTYPE, STATIC
ET,1,BEAM3
MP,EX,1,68900.000000
MP,NUXY,1,0.330000
LESIZE,ALL,,,eldiv,1
!29 real constants defining the cross-section area and moment of inertia for each element
R,1,49.250000,15.927860,1.970000
R,2,465.000000,13405.950000,18.600000
R,3,337.000000,5103.033733,13.480000
R,4,227.500000,1569.939583,9.100000
R,5,213.750000,1302.138281,8.550000
R,6,196.500000,1011.640950,7.860000
R,7,58.000000,26.014933,2.320000
R,8,143.250000,391.942744,5.730000
R,9,368.000000,6644.804267,14.720000
R,10,498.500000,16517.116217,19.940000
R,11,137.000000,342.847067,5.480000
R,12,160.750000,553.849390,6.430000
R,13,179.500000,771.137983,7.180000
R,14,126.250000,268.307552,5.050000
R,15,208.000000,1199.854933,8.320000
R,16,169.750000,652.180915,6.790000
R,17,142.750000,387.852940,5.710000
R,18,63.500000,34.139717,2.540000
R,19,93.750000,109.863281,3.750000
R,20,144.750000,404.384456,5.790000
R,21,161.000000,556.437467,6.440000
R,22,121.750000,240.627715,4.870000
R,23,110.500000,179.897683,4.420000
R,24,26.500000,2.481283,1.060000
R,25,59.500000,28.085983,2.380000
R,26,105.000000,154.350000,4.200000
R,27,85.500000,83.336850,3.420000
R,28,27.250000,2.697977,1.090000
R,29,76.250000,59.109635,3.050000
K,1,0,72.91,0
K,2,0,0,0
K,3,27.90,5.55,0
K,4,51.55,21.36,0
K,5,67.36,45.01,0
K,6,72.91,72.91,0
K,7,29.38,0,0
K,8,61.78,6.61,0
```

K,9,93.32,27.88,0
K,10,117.28,64.07,0
K,11,63.53,0,0
K,12,106.41,8.92,0
K,13,152.90,40.50,0
K,14,108.76,0,0
K,15,171.64,13.25,0
K,16,175.13,0,0
L,1,2
L,1,6
L,6,10
L,10,13
L,13,15
L,15,16
L,16,14
L,11,14
L,7,11
L,2,7
L,2,3
L,3,4
L,4,5
L,5,6
L,1,5
L,1,4
L,1,3
L,3,7
L,4,8
L,5,9
L,7,8
L,8,9
L,9,10
L,8,11
L,9,12
L,11,12
L,12,13
L,12,14
L,15,14
REAL,1
LMESH,1
REAL,2
LMESH,2
REAL,3
LMESH,3
REAL,4
LMESH,4
REAL,5
LMESH,5
REAL,6
LMESH,6
REAL,7
LMESH,7
REAL,8

```
LMESH,8
REAL,9
LMESH,9
REAL,10
LMESH,10
REAL,11
LMESH,11
REAL,12
LMESH,12
REAL,13
LMESH,13
REAL,14
LMESH,14
REAL,15
LMESH,15
REAL,16
LMESH,16
REAL,17
LMESH,17
REAL,18
LMESH,18
REAL,19
LMESH,19
REAL,20
LMESH,20
REAL,21
LMESH,21
REAL,22
LMESH,22
REAL,23
LMESH,23
REAL,24
LMESH,24
REAL,25
LMESH,25
REAL,26
LMESH,26
REAL,27
LMESH,27
REAL,28
LMESH,28
REAL,29
LMESH,29
/SOLUTION
D,23,UY,0
DL,1,,UX,0
D,1,ROTZ,0
D,2,ROTZ,0
D,3,ROTZ,0
D,4,ROTZ,0
D,5,ROTZ,0
D,6,ROTZ,0
```

```
F,1,FY,-49250.000000
SOLVE
FINISH
/POST1
 *get,nelem,elem,0,count
ETABLE,max_stress,nmisc,1
*dim,stress_1,array,nelem
*do,iel,1,nelem
*get,s,etab,1,elem,iel
stress_1(iel)= s
*enddo
/cwd,'C:\Research\ProjectMichell\Simulated_Annealing'
*CREATE, 'C:\Research\ProjectMichell\Simulated_Annealing\output1.txt'
*END
*CFOPEN,output1,TXT
*VWRITE,STRESS_1(1)
(f)
*CFCLOS
*get,nelem,elem,0,count
ETABLE,min_stress,nmisc,2
*dim,stress_2,array,nelem
*do,iel,1,nelem
*get,s,etab,2,elem,iel
stress_2(iel)= s
*enddo
/cwd,'C:\Research\ProjectMichell\Simulated_Annealing'
*CREATE, 'C:\Research\ProjectMichell\Simulated_Annealing\output2.txt'
*END
*CFOPEN,output2,TXT
*VWRITE,STRESS_2(1)
(f)
*CFCLOS
/EXIT
```

Cantilever Beam

```
FINISH
/PREP7
/TITLE, Cantilever Beam
ANTYPE, STATIC
ET,1,BEAM3
MP,EX,1,68900.000000
MP,NUXY,1,0.330000
LESIZE,ALL,,,eldiv,1
!32 real constants defining the cross-section area and moment of inertia for each element
R,1,10.10,0.8586, 1.01
R,2,15.90,3.3497, 1.59
R,3,19.00,5.7158, 1.90
R,4,14.50,2.5405, 1.45
R,5,14.10,2.3360, 1.41
R,6,13.80,2.1901, 1.38
R,7,15.00,2.8125, 1.50
```

R,8,16.80,3.9514, 1.68
R,9,15.70,3.2249, 1.57
R,10,10.10,0.8586, 1.01
R,11,10.10,0.8586, 1.01
R,12,11.20,1.1708, 1.12
R,13,11.30,1.2024, 1.13
R,14,10.40,0.9374, 1.04
R,15,10.60,0.9925, 1.06
R,16,11.20,1.1708, 1.12
R,17,10.40,0.9374, 1.04
R,18,10.10,0.8586, 1.01
R,19,11.00,1.1092, 1.10
R,20,11.50,1.2674, 1.15
R,21,12.70,1.7070, 1.27
R,22,11.10,1.1397, 1.11
R,23,12.70,1.7070, 1.27
R,24,12.80,1.7476, 1.28
R,25,10.40,0.9374, 1.04
R,26,11.40,1.2346, 1.14
R,27,10.90,1.0792, 1.09
R,28,10.10,0.8586, 1.01
R,29,10.40,0.9374, 1.04
R,30,10.30,0.9106, 1.03
R,31,10.10,0.8586, 1.01
R,32,11.10,1.1397, 1.11
R,33,30.00,22.5000, 3.00
K,1,0,0,0
K,2,-15,15,0
K,3,6.21,15,0
K,4,17.38,14.27,0
K,5,31.87,9.50,0
K,6,45,0,0
K,7,31.87,-9.50,0
K,8,17.38,-14.27,0
K,9,6.21,-15,0
K,10,-15,-15,0
K,11,5.49,9.51,0
K,12,3.37,4.39,0
K,13,3.37,-4.39,0
K,14,5.49,-9.51,0
K,15,14.88,6.73,0
K,16,10,0,0
K,17,14.88,-6.73,0
K,18,25,0,0
L,1,2
L,2,3
L,3,4
L,4,5
L,5,6
L,6,7
L,7,8
L,8,9

```
L,9,10
L,10,1
L,2,11
L,2,12
L,10,13
L,10,14
L,3,11
L,11,12
L,12,1
L,1,13
L,13,14
L,14,9
L,11,15
L,12,16
L,13,16
L,14,17
L,4,15
L,15,16
L,16,17
L,17,8
L,15,18
L,17,18
L,18,5
L,18,7
L,10,2
REAL,1
LMESH,1
REAL,2
LMESH,2
REAL,3
LMESH,3
REAL,4
LMESH,4
REAL,5
LMESH,5
REAL,6
LMESH,6
REAL,7
LMESH,7
REAL,8
LMESH,8
REAL,9
LMESH,9
REAL,10
LMESH,10
REAL,11
LMESH,11
REAL,12
LMESH,12
REAL,13
LMESH,13
REAL,14
```

```
LMESH,14
REAL,15
LMESH,15
REAL,16
LMESH,16
REAL,17
LMESH,17
REAL,18
LMESH,18
REAL,19
LMESH,19
REAL,20
LMESH,20
REAL,21
LMESH,21
REAL,22
LMESH,22
REAL,23
LMESH,23
REAL,24
LMESH,24
REAL,25
LMESH,25
REAL,26
LMESH,26
REAL,27
LMESH,27
REAL,28
LMESH,28
REAL,29
LMESH,29
 REAL,30
LMESH,30
 REAL,31
LMESH,31
REAL,32
LMESH,32
REAL,33
LMESH,33
/SOLUTION
DL,33,,ALL,0
F,22,FY,-4000.000000
SOLVE
FINISH
/POST1
*get,nelem,elem,0,count
ETABLE,Max_stress,nmisc,1
*dim,stress_1,array,nelem
*do,iel,1,nelem
*get,s,etab,1,elem,iel
stress_1(iel)= s
*enddo
```

```
/cwd,'C:\Research\Cantilever Beam\Simulated_Annealing'
*CREATE, 'C:\Research\Cantilever Beam\Simulated_Annealing\cant_output1.txt'
*END
*CFOPEN,cant_output1,txt
*VWRITE,STRESS_1(1)
(f)
*CFCLOS
*get,nelem,elem,0,count
ETABLE,Min_stress,nmisc,2
*dim,stress_2,array,nelem
*do,iel,1,nelem
*get,s,etab,2,elem,iel
stress_2(iel)= s
*enddo
/cwd,'C:\Research\Cantilever Beam\Simulated_Annealing'
*CREATE, 'C:\Research\Cantilever Beam\Simulated_Annealing\cant_output2.txt'
*END
*CFOPEN,cant_output2,txt
*VWRITE,STRESS_2(1)
(f)
*CFCLOS
/EXIT
```

C. Matlab Code

Parent Function: Simply-Supported Beam

```
clc
clear all
%Parent function using simulated annealing for truss optimization
%Al 6061 alloy: http://asm.matweb.com/search/SpecificMaterial.asp?bassnum=MA6061t6
%Constraints are have penalty factor in them
%Variable Initialization
rp=1e-1;        FOS=1;      rp_am=2;   penalty_am=0;    am_current=0;
t1=30;         no_runs=350; runs_per_iteration=30;
frac = 0.99;        % Fractional reduction every cycle
yield_strength=276;     density=2.7e-3; %g/mm^3
stress_allow=yield_strength/FOS;
function_calls=0;       penalty=0;
best_fitness=zeros(1,no_runs);  best_mass=zeros(1,no_runs);
best_thickness=zeros(29,no_runs); prev_rp=rp;
max_stress=zeros(1,no_runs);
am_violations=zeros(1,no_runs);
thicknessvalue=10*ones(29,1);
%Calculate mass, penalty and fitness of 1st design
michell_truss_objF(thicknessvalue);
stressvalue=abs(readoutput());
function_calls=function_calls+1;
volume=truss_vol(thicknessvalue);
mass=volume*density;
for i=1:29
   if stressvalue(i)>stress_allow
      penalty=penalty+(stressvalue(i)-stress_allow);
   end
end
penalty_am=check_constraint(thicknessvalue);
fitness=mass+rp*penalty + rp_am*penalty_am;
am_violations(1)=penalty_am;
best_fitness(1)=fitness;
best_mass(1)=mass;
best_thickness(:,1)=thicknessvalue;
max_stress(1)=max(stressvalue);
current_stress_max=max(stressvalue); % only a filler term if none of the if loops are entered in Line 117
tic
for iteration=2:no_runs
   fitness=mass+(fitness-mass)*rp/prev_rp; %Updating fitness based on new value of rp
   for point=1:runs_per_iteration
      penalty=0;
      new_thicknessvalue=thicknessvalue; %Generate new design
      %This section includes roulette wheel code. Only for all stresses below yield
      if max(abs(stressvalue))<stress_allow
         new_thicknessvalue=thicknessvalue; %Generate new design
         j=ceil(29*rand);
```

```
            new_thicknessvalue(j)=new_thicknessvalue(j)-0.7+rand;
           if new_thicknessvalue(j)<1 || new_thicknessvalue(j)>25
             new_thicknessvalue(j)=thicknessvalue(j);
           end
        else
        for i=1:10
           j=ceil(29*rand);
           if stressvalue(j)<stress_allow %Less than yield strength
              new_thicknessvalue(j)=thicknessvalue(j)-0.5+rand;
           else if stressvalue(j)>stress_allow
              new_thicknessvalue(j)=thicknessvalue(j)+rand;
              end
           end
           if new_thicknessvalue(j)<1|| new_thicknessvalue(j)>25
              new_thicknessvalue(j)=thicknessvalue(j);
           end
        end
        end
        michell_truss_objF(new_thicknessvalue);     new_stressvalue=abs(readoutput());
        new_stress_max=max(new_stressvalue);        function_calls=function_calls+1;
        new_volume=truss_vol(new_thicknessvalue);   new_mass=new_volume*density;
for i=1:29
   if new_stressvalue(i)>stress_allow
      penalty=penalty+(new_stressvalue(i)-stress_allow);
   end
end
 penalty_am=check_constraint(thicknessvalue);
new_fitness=new_mass+rp*penalty + rp_am*penalty_am;
delta_e=fitness-new_fitness;
 if delta_e>=0
   thicknessvalue=new_thicknessvalue;  stressvalue=new_stressvalue;
   fitness=new_fitness;              mass=new_mass;
   current_stress_max=new_stress_max;  am_current=penalty_am;
 else if delta_e<0
       p=exp((delta_e)/t1);
       r=rand;
       if r<p
          fitness=new_fitness;              mass=new_mass;
          thicknessvalue=new_thicknessvalue;  current_stress_max=new_stress_max;
          am_current=penalty_am;            stressvalue=new_stressvalue;
       end
   end
end
   end
      best_fitness(iteration)=fitness; best_mass(iteration)=mass;
   best_thickness(:,iteration)=thicknessvalue;
   max_stress(iteration)=current_stress_max;
   am_violations(iteration)=am_current;
   t1=t1*frac;
   prev_rp=rp;
   rp=iteration/10;
   plot(best_fitness)
```

```
end
toc
plot(best_fitness,'b')
legend('fitness vs iterations')
xlabel('iterations')
ylabel('fitness')
```

ANSYS Input File Creation

```
function [ ] = michell_truss_objF(thicknessvalue)
%This function will receive thickness values as an input and run it in
%ANSYS. An output file will be written in the respective directory
num_of_elements=length(thicknessvalue);
%Syntax to start writing a file
%Link for material values: http://asm.matweb.com/search/SpecificMaterial.asp?bassnum=MA6061t6
% ansys file names
ansys_file_title='Michell Truss';
ansys_output_location='"C:\Research\ProjectMichell\Simulated_Annealing"';
ansys_output_file1='"C:\Research\ProjectMichell\Simulated_Annealing\output1.txt"';
ansys_output_file2='"C:\Research\ProjectMichell\Simulated_Annealing\output2.txt"';
%ansys_path: CHANGE MANUALLY;
%ansys_input_path: CHANGE MANUALLY;;
%ansys constants
elastic_modulus=6.89e4; % E for 6061 Al alloy
poisson_ratio=0.33;
force=-49250;
depth=25;
fclose('all');
      %Syntax to start writing a file
       fname=('truss_model.txt');
       fid=fopen(fname,'w+');
  %File commands written inside text file created above
       fprintf(fid,'FINISH\r\n');
       fprintf(fid,'/PREP7\r\n');
       fprintf(fid,'/TITLE, %s \r\n', ansys_file_title);
  fprintf(fid,'ANTYPE, STATIC \r\n');
       fprintf(fid,'ET,1,BEAM3 \r\n');
       fprintf(fid,'MP,EX,1,%f \r\n',elastic_modulus);
       fprintf(fid,'MP,NUXY,1,%f\r\n',poisson_ratio);
       fprintf(fid,'LESIZE,ALL,,,eldiv,1\r\n\r\n');
       fprintf(fid,'!29 real constants defining the cross-section area and moment of inertia for each element\r\n
\r\n');
     %Calculating 29 Real constants
       for i=1:num_of_elements
```

```
    area(i)=depth*thicknessvalue(i);
    MOI(i)=depth*(thicknessvalue(i)^3)/12;
 fprintf(fid,'R,%i,%5.6f,%5.6f,%5.6f \r\n',i,area(i),MOI(i),thicknessvalue(i));
 end
 fprintf(fid,'\r\nK,1,0,72.91,0\r\n');
 fprintf(fid,'K,2,0,0,0\r\n');
 fprintf(fid,'K,3,27.90,5.55,0\r\n');
 fprintf(fid,'K,4,51.55,21.36,0\r\n');
 fprintf(fid,'K,5,67.36,45.01,0\r\n');
 fprintf(fid,'K,6,72.91,72.91,0\r\n');
 fprintf(fid,'K,7,29.38,0,0\r\n');
 fprintf(fid,'K,8,61.78,6.61,0\r\n');
 fprintf(fid,'K,9,93.32,27.88,0\r\n');
 fprintf(fid,'K,10,117.28,64.07,0\r\n');
 fprintf(fid,'K,11,63.53,0,0\r\n');
 fprintf(fid,'K,12,106.41,8.92,0\r\n');
 fprintf(fid,'K,13,152.90,40.50,0\r\n');
 fprintf(fid,'K,14,108.76,0,0\r\n');
 fprintf(fid,'K,15,171.64,13.25,0\r\n');
 fprintf(fid,'K,16,175.13,0,0\r\n \r\n');
 fprintf(fid,'L,1,2 \r\n');
 fprintf(fid,'L,1,6 \r\n');
 fprintf(fid,'L,6,10 \r\n');
 fprintf(fid,'L,10,13 \r\n');
 fprintf(fid,'L,13,15 \r\n');
fprintf(fid,'L,15,16 \r\n');
 fprintf(fid,'L,16,14 \r\n');
 fprintf(fid,'L,11,14 \r\n');
 fprintf(fid,'L,7,11 \r\n');
 fprintf(fid,'L,2,7 \r\n');
fprintf(fid,'L,2,3 \r\n');
 fprintf(fid,'L,3,4 \r\n');
 fprintf(fid,'L,4,5 \r\n');
 fprintf(fid,'L,5,6 \r\n');
 fprintf(fid,'L,1,5 \r\n');
fprintf(fid,'L,1,4 \r\n');
 fprintf(fid,'L,1,3 \r\n');
 fprintf(fid,'L,3,7 \r\n');
 fprintf(fid,'L,4,8 \r\n');
 fprintf(fid,'L,5,9 \r\n');
fprintf(fid,'L,7,8 \r\n');
 fprintf(fid,'L,8,9 \r\n');
 fprintf(fid,'L,9,10 \r\n');
 fprintf(fid,'L,8,11 \r\n');
 fprintf(fid,'L,9,12 \r\n');
```

```
fprintf(fid,'L,11,12 \r\n');
fprintf(fid,'L,12,13 \r\n');
fprintf(fid,'L,12,14 \r\n');
fprintf(fid,'L,15,14 \r\n\r\n');
for i=1:29
   fprintf(fid,'REAL,%i \r\n',i);
   fprintf(fid,'LMESH,%i \r\n \r\n',i);
end
fprintf(fid,'/SOLUTION \r\n');
fprintf(fid,'D,23,UY,0 \r\n');
fprintf(fid,'DL,1,,UX,0 \r\n \r\n');
fprintf(fid,'D,1,ROTZ,0 \r\n');
fprintf(fid,'D,2,ROTZ,0 \r\n');
fprintf(fid,'D,3,ROTZ,0 \r\n');
fprintf(fid,'D,4,ROTZ,0 \r\n');
fprintf(fid,'D,5,ROTZ,0 \r\n');
fprintf(fid,'D,6,ROTZ,0 \r\n');
fprintf(fid,'F,1,FY,%f \r\n',force);
fprintf(fid,'SOLVE \r\n');
fprintf(fid,'FINISH \r\n');
%postprocessing code
fprintf(fid,'/POST1 \r\n \r\n');
%OUTPUT1
fprintf(fid,'*get,nelem,elem,0,count \r\n\r\n');
fprintf(fid,'ETABLE,max_stress,nmisc,1 \r\n\r\n');
fprintf(fid,'*dim,stress_1,array,nelem \r\n\r\n');
fprintf(fid,'*do,iel,1,nelem \r\n');
fprintf(fid,'*get,s,etab,1,elem,iel \r\n');
fprintf(fid,'stress_1(iel)= s \r\n');
fprintf(fid,'*enddo \r\n');
fprintf(fid,'/cwd,%s \r\n',ansys_output_location);
fprintf(fid,'*CREATE, %s \r\n',ansys_output_file1);
fprintf(fid,'*END\r\n');
fprintf(fid,'*CFOPEN,output1,TXT \r\n');
fprintf(fid,'*VWRITE,STRESS_1(1) \r\n');
fprintf(fid,'(f) \r\n');
fprintf(fid,'*CFCLOS \r\n');
 %OUTPUT2
fprintf(fid,'*get,nelem,elem,0,count \r\n\r\n');
fprintf(fid,'ETABLE,min_stress,nmisc,2 \r\n\r\n');
fprintf(fid,'*dim,stress_2,array,nelem \r\n\r\n');
fprintf(fid,'*do,iel,1,nelem \r\n');
fprintf(fid,'*get,s,etab,2,elem,iel \r\n');
fprintf(fid,'stress_2(iel)= s \r\n');
fprintf(fid,'*enddo \r\n');
```

```
        fprintf(fid,'/cwd,%s \r\n',ansys_output_location);
        fprintf(fid,'*CREATE, %s \r\n',ansys_output_file2);
        fprintf(fid,'*END\r\n');
        fprintf(fid,'*CFOPEN,output2,TXT \r\n');
        fprintf(fid,'*VWRITE,STRESS_2(1) \r\n');
        fprintf(fid,'(f) \r\n');
        fprintf(fid,'*CFCLOS \r\n');
        fprintf(fid,'/EXIT \r\n');
        fclose(fid);
  dos('"C:\Program Files\ANSYS Inc\v150\ansys\bin\winx64\ANSYS150" -i
"C:\Research\ProjectMichell\Simulated_Annealing\truss_model.txt"');
  end
```

Stress Calculation

```
function [ stressvalue ] = readoutput()
%function to store unique output values
%A is another temporary variable to store stress in it's sym form
fileID = fopen('output1.txt','r');
formatspec='%f';
tempstressvalue=(fscanf(fileID,formatspec)); %stores all file values in variable
A=zeros(29,1);
for i=1:202
    tempstressvalue(i)=abs(round(tempstressvalue(i)*1e4)/1e4);
end
%These array values represent the start and finish element numbers for each
%line
array_1=[1 6 11 15 18 22 25 40 55 70 76 82 90 94 97 102 107 115 118 ...
    122 126 141 149 153 156 161 176 185 188];
array_2=[5 10 14 17 21 24 39 54 69 75 81 89 93 96 101 106 114 117 ...
    121 125 140 148 152 155 160 175 184 187 202];
for i=1:29
    A(i)=tempstressvalue(array_1(i));
    for j=array_1(i)+1:array_2(i)
        if tempstressvalue(j)>A(i)
            A(i)=tempstressvalue(j);
        end
    end
end
%_____________________ 2nd stress reading_____________________________
fileID = fopen('output2.txt','r');
formatspec='%f';
tempstressvalue=(fscanf(fileID,formatspec));
B=zeros(29,1);
for i=1:202
```

```
   tempstressvalue(i)=abs(round(tempstressvalue(i)*1e4)/1e4);
end
%All values are unique
array_1=[1 6 11 15 18 22 25 40 55 70 76 82 90 94 97 102 107 115 118 ...
   122 126 141 149 153 156 161 176 185 188];
array_2=[5 10 14 17 21 24 39 54 69 75 81 89 93 96 101 106 114 117 ...
   121 125 140 148 152 155 160 175 184 187 202];
for i=1:29
   B(i)=tempstressvalue(array_1(i));
   for j=array_1(i)+1:array_2(i)
      if tempstressvalue(j)>B(i)
         B(i)=tempstressvalue(j);
      end
   end
end
for i=1:29
   stressvalue(i)=max(A(i),B(i));
end
end
```

Volume Calculation

```
function [volume]=truss_vol(thickness)
depth=25;
volume=0; %Initial Volume
K=[0 72.91; 0 0; 27.90 5.55; 51.515 21.36; 67.36 45.01; 72.91 72.91; 29.38 0; 61.78 6.61; 93.32 27.88;...
125.47 68.55; 67.96 0; 113.84 9.54; 163.57 40.50; 108.76 0; 171.64 13.25; 175 0];
DL(1)=sqrt( (K(2,1)-K(1,1))^2 + (K(2,2)-K(1,2))^2 );
DL(2)=sqrt( (K(6,1)-K(1,1))^2 + (K(6,2)-K(1,2))^2 );
DL(3)=sqrt( (K(10,1)-K(6,1))^2 + (K(10,2)-K(6,2))^2 );
DL(4)=sqrt( (K(13,1)-K(10,1))^2 + (K(13,2)-K(10,2))^2 );
DL(5)=sqrt( (K(13,1)-K(15,1))^2 + (K(13,2)-K(15,2))^2 );
DL(6)=sqrt( (K(15,1)-K(16,1))^2 + (K(15,2)-K(16,2))^2 );
DL(7)=sqrt( (K(16,1)-K(14,1))^2 + (K(16,2)-K(14,2))^2 );
DL(8)=sqrt( (K(11,1)-K(14,1))^2 + (K(11,2)-K(14,2))^2 );
DL(9)=sqrt( (K(7,1)-K(11,1))^2 + (K(7,2)-K(11,2))^2 );
DL(10)=sqrt( (K(2,1)-K(7,1))^2 + (K(2,2)-K(7,2))^2 );
DL(11)=sqrt( (K(2,1)-K(3,1))^2 + (K(2,2)-K(3,2))^2 );
DL(12)=sqrt( (K(3,1)-K(4,1))^2 + (K(3,2)-K(4,2))^2 );
DL(13)=sqrt( (K(4,1)-K(5,1))^2 + (K(4,2)-K(5,2))^2 );
DL(14)=sqrt( (K(5,1)-K(6,1))^2 + (K(5,2)-K(6,2))^2 );
DL(15)=sqrt( (K(1,1)-K(5,1))^2 + (K(1,2)-K(5,2))^2 );
DL(16)=sqrt( (K(1,1)-K(4,1))^2 + (K(1,2)-K(4,2))^2 );
DL(17)=sqrt( (K(1,1)-K(3,1))^2 + (K(1,2)-K(3,2))^2 );
```

```
DL(18)=sqrt( (K(3,1)-K(7,1))^2 + (K(3,2)-K(7,2))^2 );
DL(19)=sqrt( (K(4,1)-K(8,1))^2 + (K(4,2)-K(8,2))^2 );
DL(20)=sqrt( (K(5,1)-K(9,1))^2 + (K(5,2)-K(9,2))^2 );
DL(21)=sqrt( (K(7,1)-K(8,1))^2 + (K(7,2)-K(8,2))^2 );
DL(22)=sqrt( (K(8,1)-K(9,1))^2 + (K(8,2)-K(9,2))^2 );
DL(23)=sqrt( (K(9,1)-K(10,1))^2 + (K(9,2)-K(10,2))^2 );
DL(24)=sqrt( (K(11,1)-K(8,1))^2 + (K(8,2)-K(11,2))^2 );
DL(25)=sqrt( (K(12,1)-K(9,1))^2 + (K(12,2)-K(9,2))^2 );
DL(26)=sqrt( (K(11,1)-K(12,1))^2 + (K(11,2)-K(12,2))^2 );
DL(27)=sqrt( (K(12,1)-K(13,1))^2 + (K(12,2)-K(13,2))^2 );
DL(28)=sqrt( (K(14,1)-K(12,1))^2 + (K(14,2)-K(12,2))^2 );
DL(29)=sqrt( (K(15,1)-K(14,1))^2 + (K(15,2)-K(14,2))^2 );

for i=1:29
volume= volume+ DL(i)*thickness(i)*depth;
end
```

AM Constraint for Simply-Supported Beam

```
function [p1] = check_constraint(t)
p1=0;
%Alpha Lines
if 32.7 - ((t(18)+t(19))/2) <= 0.5  %1
   p1=p1+1;
end
if 35.2 - ((t(19)+t(20))/2) <= 0.5  %2
   p1=p1+1;
end
if 37.9 - ((t(20)+t(3))/2) <= 0.5  %3
   p1=p1+1;
end
if 43.4 - ((t(24)+t(25))/2) <= 0.5  %4
   p1=p1+1;
end
if 54.1 - ((t(25)+t(4))/2) <= 0.5  %5
   p1=p1+1;
end
if 63.4 - ((t(5)+t(28))/2) <= 0.5  %6
   p1=p1+1;
end
%Beta lines
if 12 - ((t(21)+t(12))/2) <= 0.5  %1
   p1=p1+1;
end
if 15.73 - ((t(26)+t(22))/2) <= 0.5  %2
   p1=p1+1;
end
```

```
if 26.11 - ((t(22)+t(13))/2) <= 0.5  %3
   p1=p1+1;
end
if 21.4 - ((t(29)+t(27))/2) <= 0.5  %4
   p1=p1+1;
end
if 34.5 - ((t(27)+t(23))/2) <= 0.5  %5
   p1=p1+1;
end
if 41.1 - ((t(23)+t(14))/2) <= 0.5  %6
   p1=p1+1;
end
```